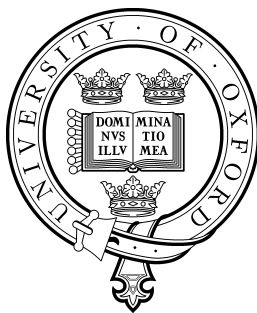


# Flow Excitation of a Finite Curved Elastic Shell



Gareth Wyn Jones  
Jesus College  
University of Oxford

A dissertation submitted in partial fulfillment of the degree of  
*Master of Science*  
*in*  
*Mathematical Modelling and Scientific Computing*

Summer 2003

## **Acknowledgements**

I would like to thank my project supervisor, Dr David Allwright, for all the guidance and assistance he has given me over the past few months. In addition, I am indebted to Thales Underwater Systems for suggesting the problem, for supplying relevant information about the sonar dome properties, and for their support of the MSc fund, making possible a generous bursary which has sustained me for the project's duration.

## Abstract

This dissertation investigates the vibrations and acoustics of a particular type of sonar array, in which the hydrophone array is attached to the hull of the ship and is protected from the external flow by a sonar dome, with a free-flooding space between the dome and the array. When the ship moves through the water, a turbulent boundary layer forms over the sonar dome, and the pressure fluctuations in this cause vibrations of the dome and sound waves in the water between the dome and the array. In some circumstances the array detects these waves as appearing to originate at certain bearings either side of end-fire, degrading the array's performance. It has been suggested that this effect is due to longitudinal wave motion in the sonar dome. To investigate the validity of this claim, and to suggest other possible explanations, various simplified models of the problem are considered, treating the sonar dome as an infinite thick plate, an infinitely long cylindrical shell, and a finite thin plate. Acoustic resonances in the water between the dome and the array are also considered.

# Contents

<b>1</b>	<b>Introduction</b>	<b>1</b>
1.1	Interpretation of the Noise Signals . . . . .	2
<b>2</b>	<b>Thick Plate Motion</b>	<b>7</b>
2.1	Motion of the Plate: Impedance and Free Motion . . . . .	7
2.2	Motion with Fluid Loading . . . . .	11
2.3	Impedances . . . . .	14
2.4	Thin Plate Approximation . . . . .	15
2.5	Thick Plate with a Rigid Boundary . . . . .	16
2.6	Discussion . . . . .	17
<b>3</b>	<b>Analysis of an Infinite Cylindrical Shell</b>	<b>19</b>
3.1	Thin Cylindrical Shell . . . . .	19
3.1.1	Motion with Fluid Loading . . . . .	21
3.1.2	Inclusion of a Rigid Cylinder . . . . .	23
3.2	Infinite Thick Cylindrical Shell . . . . .	24
3.2.1	Free Motion . . . . .	25
3.2.2	Water-filled Hollow Cylinder . . . . .	30
3.2.3	Inclusion of a Rigid Cylinder . . . . .	31
3.3	Results and Discussion . . . . .	32
<b>4</b>	<b>Effects of a Finite Plate</b>	<b>33</b>
4.1	Analysis of a Finite Plate . . . . .	33
4.1.1	Problem Formulation . . . . .	33
4.1.2	The Finite Difference Method . . . . .	35
4.1.3	Inclusion of a Rigid Boundary . . . . .	37
4.2	An Alternative Method . . . . .	38
4.3	Results and Discussion . . . . .	40

<b>5</b>	<b>Viscoelastic Effects</b>	<b>42</b>
5.1	The Complex Modulus . . . . .	42
5.2	Results and Discussion . . . . .	43
<b>6</b>	<b>Conclusions</b>	<b>45</b>
6.1	Interpretation of the Results . . . . .	45
6.2	Further Research . . . . .	46
<b>A</b>	<b>Graphs</b>	<b>47</b>
	<b>References</b>	<b>67</b>

# List of Figures

1.1	The free-flooding structure, depicting the sonar dome . . . . .	1
1.2	Approximate geometry of the sonar dome . . . . .	3
1.3	Dimensions of the bottom edge of the sonar dome . . . . .	3
1.4	Connection of the sonar dome to the free-flooding structure . . . . .	4
1.5	Wavefronts approaching the hydrophones . . . . .	4
1.6	Wavefronts approaching $CD$ . . . . .	5
2.1	Symmetric and antisymmetric modes of motion . . . . .	10
2.2	The infinite thick plate with fluid loading . . . . .	11
2.3	Thick plate with a rigid boundary . . . . .	16
3.1	Cylindrical coordinates . . . . .	20
3.2	Cylindrical shell with rigid cylinder . . . . .	24
3.3	Diagram of the thick cylindrical tube . . . . .	28
3.4	Diagram of the thick cylindrical tube with a rigid cylinder . . . . .	31
4.1	A finite plate . . . . .	33
4.2	Grid for the numerical scheme . . . . .	36
A.1	Graph of the pressure on the lower side of a thin plate . . . . .	47
A.2	Graph of the pressure on the lower side of a thick plate . . . . .	48
A.3	Graph of the pressure from a thin plate with a rigid boundary . . . . .	49
A.4	Thick plate rigid boundary comparison graph . . . . .	50
A.5	Graph of the pressure inside of a thin cylindrical shell . . . . .	51
A.6	Graph of the pressure inside a thin cylindrical shell on a rigid cylinder . . . . .	52
A.7	Graph of the pressure inside a thick cylindrical shell . . . . .	53
A.8	Graph of the pressure inside a thick cylindrical shell on a rigid cylinder . . . . .	54
A.9	Graph of the pressure behind a thin finite plate . . . . .	55
A.10	Graph of the pressure behind a thin finite plate at $k = 33.99 \text{ m}^{-1}$ . . . . .	56
A.11	Graph of the pressure behind a thin finite plate at $k = 33.99 \text{ m}^{-1}$ . . . . .	56

A.12 Graph of the thin finite plate displacement at $k = 33.99 \text{ m}^{-1}$ . . . . .	57
A.13 Graph of the pressure behind a thin finite plate with a rigid boundary . . . . .	58
A.14 Graph of the pressure behind a thin finite plate at $k = 33.99 \text{ m}^{-1}$ . . . . .	59
A.15 Graph of the pressure behind a thin finite plate at $k = 33.99 \text{ m}^{-1}$ . . . . .	59
A.16 Graph of the thin finite plate displacement with a rigid boundary at $k = 33.99 \text{ m}^{-1}$ .	60
A.17 Graph of the pressure on the lower side of a thick plate with complex elastic moduli	61
A.18 Thick plate rigid boundary comparison graph with complex elastic moduli . . . . .	62
A.19 Graph of the pressure inside a thin cylindrical shell with complex elastic moduli . .	63
A.20 Graph of the pressure inside a thick cylindrical shell with complex elastic moduli . .	64
A.21 Graph of the pressure behind a thin finite plate with complex elastic moduli . . . . .	65
A.22 Graph of a thin finite plate with a rigid boundary and complex elastic moduli . . . . .	66

# Chapter 1

## Introduction

This project will deal with sonar arrays mounted on the hull of a ship. The array itself is comprised of several hydrophones which are arranged in vertical staves. These are housed in a free-flooding structure which is then attached to the ship's hull. This free-flooding structure is not an integral part of the hull, so it can be filled with water. To allow acoustic signals to propagate to the array, an 'acoustic window' needs to be incorporated into the structure, as depicted in Figure 1.1. This window often comprises a 'sonar dome', which allows signals to pass through with minimum attenuation. The array is then mounted within the free-flooding structure and placed in the still water behind the dome, at an offset of  $h_0$ . As the ship travels through the sea, a turbulent boundary layer will build

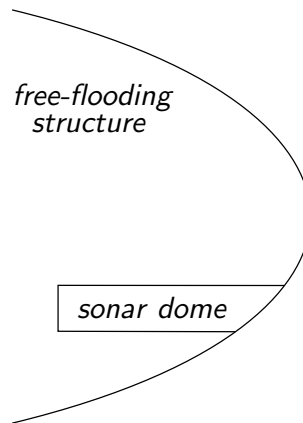


Figure 1.1: The free-flooding structure, depicting the sonar dome

up over the dome, from a stagnation point at the very front of the structure. Noise in this turbulent boundary layer will travel through the sonar dome and the still water towards the hydrophones.

It is found that when the ship travels above a certain speed, the sonar array detects noise appearing to come from certain headings either side of end-fire — that is, either side of the direction in which the ship is travelling. The noise appears in a relatively wide range of angles near this heading, which for some shapes of sonar dome can be about  $45^\circ$ . In this project we aim to understand

the vibration field set up by the boundary layer noise, and why it appears to the sonar at these angles.

The sonar dome is made of a material called glass reinforced plastic (GRP), whose properties are given in Table 1.1. Initially we will treat the material as isotropic and perfectly elastic. Here  $\rho_p$  is the density and  $\lambda$  and  $\mu$  are the Lamé constants.

Table 1.1: GRP Properties

Property	Value
$\rho_p$	$1650 \text{ kg m}^{-3}$
$\lambda$	$6.28 \times 10^9 \text{ Pa}$
$\mu$	$3.24 \times 10^9 \text{ Pa}$

In this project, we are interested in noise and vibrations at frequencies of several kHz. As a representative frequency for use in calculations, we shall often take  $f = 5 \text{ kHz}$ . At these frequencies the GRP dissipates energy slightly. If this effect becomes important, we shall take  $\lambda$  and  $\mu$  to be complex with argument  $\delta$  given by  $\tan \delta = 0.01$ .

In practice the sonar dome is conformal to the free-flooding structure, and hence can be regarded as two rectangular sections joined by a central part that is approximately a section of a cone. We shall here neglect the deviation of the surface from vertical, and therefore regard it as two vertical rectangles joined by an arc of a cylinder, as in Figure 1.2. Rough values for the sonar dome's dimensions are given in Table 1.2, with reference to Figures 1.2 and 1.3 (exact values cannot be given). The thickness is represented by  $h$ . Finally, we note that the sonar dome is connected to the free-flooding structure as shown in Figure 1.4.

Table 1.2: Sonar Dome Dimensions

Dimension	Value
$a$	10 m
$b$	3 m
$R$	5 m
$h$	0.05 m
$h_0$	0.25 m
$\alpha$	$25^\circ$

## 1.1 Interpretation of the Noise Signals

Before we attempt to explain the origin of the noise, we will give an interpretation of its appearing to originate from one particular direction. Consider waves approaching the hydrophones at an angle  $\theta_0$  from end-fire, as shown in Figure 1.5.

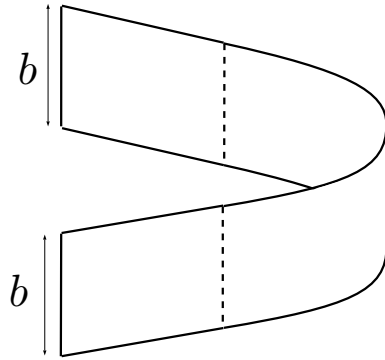


Figure 1.2: Approximate geometry of the sonar dome

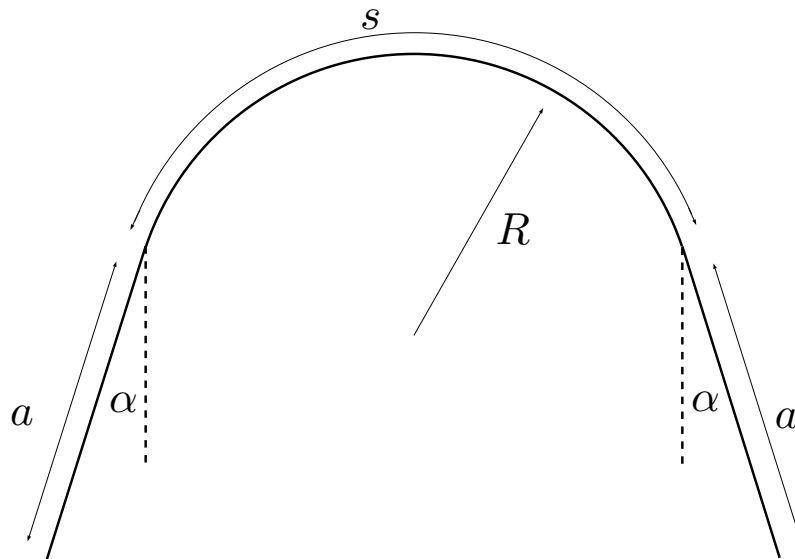


Figure 1.3: Dimensions of the bottom edge of the sonar dome

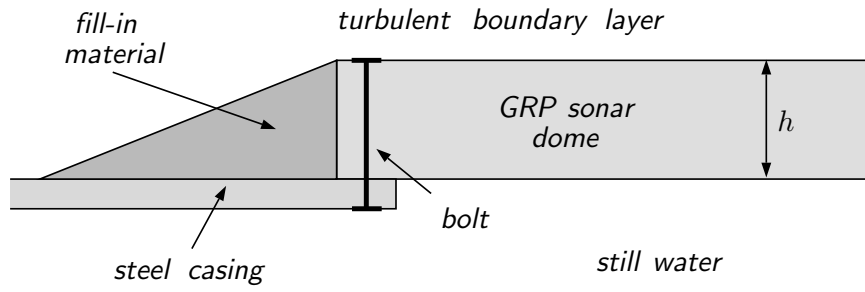


Figure 1.4: Connection of the sonar dome to the free-flooding structure

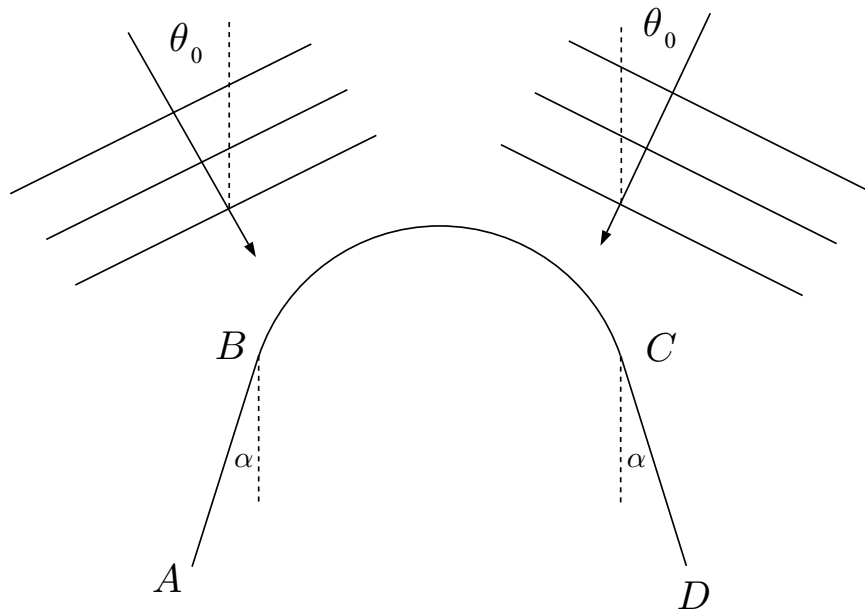


Figure 1.5: Wavefronts approaching the hydrophones

The sonar array, in detecting sounds from one direction, only uses the hydrophones on that side of the array. So, if a signal were approaching from the right, the signal would be detected by the hydrophones on  $CD$  and on most of  $BC$ .

Consider the section  $CD$ , with the  $x$ -direction defined to be in the direction  $CD$  and  $z$  defined to be perpendicular to  $x$ , outwards into the water. Waves approaching  $CD$  at an angle  $\theta_0$  to end-fire will approach at an angle  $\theta_1 = 90^\circ - \alpha - \theta_0$  to the  $z$ -direction, as shown in Figure 1.6.

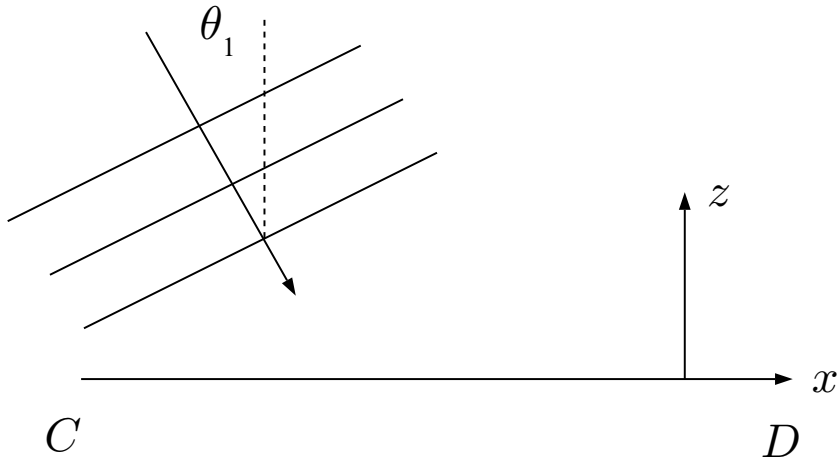


Figure 1.6: Wavefronts approaching  $CD$

Now, sound waves travelling through an acoustic medium — water, in this case — consist of pressure fluctuations  $p$  that satisfy the wave equation,

$$\nabla^2 p - \frac{1}{c_0^2} \frac{\partial^2 p}{\partial t^2} = 0 \quad (1.1)$$

where  $c_0$  is the speed of sound in the medium (see Acheson [2] for instance). We assume that this pressure will be of the form

$$p = \Re(\hat{p}(x, z)e^{-i\omega t}) \quad (1.2)$$

where  $\Re$  denotes the real part. Henceforth we shall assume this convention for all quantities used in calculations. Then, the wave equation becomes

$$\nabla^2 \hat{p} + \left(\frac{\omega}{c_0}\right)^2 \hat{p} = 0 \quad (1.3)$$

or, on simplifying the notation,

$$\nabla^2 p + k_0^2 p = 0 \quad (1.4)$$

where  $k_0 = \omega/c_0$  is the fluid acoustic wavenumber. Equation (1.4) is known as the Helmholtz equation.

The solution of this equation that represents incoming waves at an angle  $\theta_1$  to the  $z$ -axis, as in Figure 1.6, is

$$p = p_0 e^{i\mathbf{k}\cdot\mathbf{x}} \quad (1.5)$$

where  $\mathbf{x} = (x, z)$  and

$$\mathbf{k} = k_0(\sin \theta_1, -\cos \theta_1) \quad . \quad (1.6)$$

Analysis of the noise appearing at  $\theta_0$  from end-fire has shown that it is consistent with a value of  $k_0 \sin \theta_1 \approx 13 \text{ m}^{-1}$ , which is the value of the *longitudinal wavenumber* of a vibrating plate of GRP. The aim of this project is to discover whether vibrations at this wavenumber are transmitted more strongly through the material and the water behind than at other wavenumbers, and whether this is due to longitudinal vibrations or some other mechanism. The vibration amplitudes are small, so we will use *linear* elasticity and acoustics throughout the project.

Firstly we will explore the theory of infinite plates, and try to discover the strength of the effect due to longitudinal motion. We will also investigate the effect of a rigid boundary at a distance  $h_0$  behind the plate, to simulate the acoustic interaction of the dome and water with the array and hull behind.

It is known that in curved shells, the curvature provides a mechanism for the coupling of transverse and longitudinal modes of motion. Therefore, in order to examine the effect of the sonar dome's curvature, we intend to look at the theories of infinite thin cylindrical shells and infinite thick cylindrical tubes, and discover whether vibrations at longitudinal wavenumbers are strongly transmitted. We will also look at the case where a rigid cylinder is included inside the shell or tube, once again to investigate the interaction with the array.

Thirdly, we aim to establish whether the edge constraints of the sonar dome have an effect on the vibration transmitted to the hydrophones, by considering a finite thin plate, attached to a rigid boundary.

Finally we will assess the validity of the different possible explanations for the increased noise levels when the slightly viscoelastic property of the material is accounted for.

All graphs and numerical procedures in this project are drawn by, or executed in, the Matlab package.

## Chapter 2

# Thick Plate Motion

We will begin our analysis by considering the excitation of a thick flat isotropic plate. Initially we will consider the free motion of the plate, before considering the effect that the presence of fluid has on the plate's motion. We will also consider the impedances of this motion, and later compare this thick plate motion with thin plate motion. In both thick-plate and thin-plate motion, the same thickness of plate,  $h$ , is used for calculations, but for the thin plate motion  $h$  is assumed small compared to the elastic wavelengths in the material. This is something that will also apply to thick and thin shell theories when they are considered later.

The thick plate has been considered by Rayleigh [15], and similar work to the fluid loading problem has been carried out before — see, for example, Brekhovskikh [4], Cremer, Heckl and Ungar [5], Junger and Feit [8] or Skelton and James [17] — but none of these directly answers the situation under consideration here, and we will consider the problem from a simpler perspective.

Finally in this chapter we shall consider the effect that a rigid boundary at a distance  $h_0$  from the plate has on the pressure in the fluid.

### 2.1 Motion of the Plate: Impedance and Free Motion

We consider an infinite plate of thickness  $h = 2H$  lying in  $-H \leq z \leq H$ . We assume that the plate is subject to applied pressures on  $z = \pm H$  which vary proportionally to  $e^{ikx}e^{-i\omega t}$ . Then, by linearity, all variables will have this same  $x$  and  $t$ -dependence. So we write the displacements of a small element of the plate as

$$\begin{pmatrix} u_x \\ u_y \\ u_z \end{pmatrix} = \begin{pmatrix} u(z) \\ v(z) \\ w(z) \end{pmatrix} e^{ikx} e^{-i\omega t} \quad (2.1)$$

for  $|z| \leq H$ . We will assume that the motion has no  $y$ -dependence.

In basic linear elasticity theory, the strain tensor is given by

$$e_{ij} = \frac{1}{2} \left( \frac{\partial u_i}{\partial x_j} + \frac{\partial u_j}{\partial x_i} \right) \quad (2.2)$$

so

$$\begin{pmatrix} e_{xx} \\ e_{xy} \\ e_{xz} \\ e_{yy} \\ e_{yz} \\ e_{zz} \end{pmatrix} = \begin{pmatrix} iku(z) \\ \frac{1}{2}ikv(z) \\ \frac{1}{2}(ikw(z) + u'(z)) \\ 0 \\ \frac{1}{2}v'(z) \\ w'(z) \end{pmatrix} e^{ikx} e^{-i\omega t} . \quad (2.3)$$

The fundamental relation between the stress tensor  $\sigma_{ij}$  and the strain tensor is given by (see, for example, Landau and Lifshitz [9])

$$\sigma_{ij} = \lambda (e_{xx} + e_{yy} + e_{zz}) \delta_{ij} + 2\mu e_{ij} \quad (2.4)$$

where  $\lambda$  and  $\mu$  are the Lamé constants, so that

$$\begin{pmatrix} \sigma_{xx} \\ \sigma_{xy} \\ \sigma_{xz} \\ \sigma_{yy} \\ \sigma_{yz} \\ \sigma_{zz} \end{pmatrix} = \begin{pmatrix} \lambda(iku(z) + w'(z)) + 2i\mu ku(z) \\ i\mu kv(z) \\ \mu(ikw(z) + u'(z)) \\ \lambda(iku(z) + w'(z)) \\ \mu v'(z) \\ \lambda(iku(z) + w'(z)) + 2\mu w'(z) \end{pmatrix} e^{ikx} e^{-i\omega t} \quad (2.5)$$

by equation (2.3).

The free-motion equation of motion for the solid is given by

$$\rho_p \frac{\partial^2 u_i}{\partial t^2} = \frac{\partial \sigma_{ij}}{\partial x_j} \quad (2.6)$$

using the summation convention. Taking  $i = 1, 2, 3$  in turn, we get the equations of motion for  $u$ ,  $v$  and  $w$ :

$$\mu u'' = ((\lambda + 2\mu)k^2 - \rho_p \omega^2) u - ik(\lambda + \mu)w' \quad (2.7)$$

$$v'' = \left( k^2 - \frac{\rho_p \omega^2}{\mu} \right) v \quad (2.8)$$

$$(\lambda + 2\mu)w'' = (\mu k^2 - \rho_p \omega^2)w - ik(\lambda + \mu)u' . \quad (2.9)$$

At this point we remind ourselves that the compressional wavespeed  $c_p$  and the shear wavespeed  $c_s$  are given by

$$c_p^2 = \frac{\lambda + 2\mu}{\rho_p} \quad (2.10)$$

$$c_s^2 = \frac{\mu}{\rho_p} \quad (2.11)$$

with associated compressional wavenumber  $k_c$  and shear wavenumber  $k_s$ :

$$k_c = \frac{\omega}{c_p} \quad (2.12)$$

$$k_s = \frac{\omega}{c_s} . \quad (2.13)$$

We shall also define at this point the plate compressional-wave normal propagation parameter,  $\nu_c = \sqrt{k^2 - k_c^2}$  and the plate shear-wave normal propagation parameter,  $\nu_s = \sqrt{k^2 - k_s^2}$  — we will comment on the sign of these quantities later.

With this notation, the equations (2.7), (2.8) and (2.9) become, respectively,

$$c_s^2 u'' = c_p^2 \nu_c^2 u - ik(c_p^2 - c_s^2)w' \quad (2.14)$$

$$v'' = \nu_s^2 v \quad (2.15)$$

$$c_p^2 w'' = c_s^2 \nu_s^2 w - ik(c_p^2 - c_s^2)u' \quad (2.16)$$

Trying a solution of the form  $u = u_0 e^{\gamma z}$ , and similarly for  $v$  and  $w$ , gives a general solution

$$u = A_1 \cosh \nu_s z + B_1 \sinh \nu_s z + C_1 \cosh \nu_c z + D_1 \sinh \nu_c z \quad (2.17)$$

$$v = A_2 \cosh \nu_s z + B_2 \sinh \nu_s z \quad (2.18)$$

$$w = A_3 \cosh \nu_s z + B_3 \sinh \nu_s z + C_3 \cosh \nu_c z + D_3 \sinh \nu_c z \quad (2.19)$$

with  $A_3, B_3, C_3$  and  $D_3$  related to  $A_1, B_1, C_1$  and  $D_1$  by equations (2.20) and (2.21):

$$\begin{pmatrix} A_3 \\ B_3 \end{pmatrix} = -\frac{ik}{\nu_s} \begin{pmatrix} B_1 \\ A_1 \end{pmatrix} \quad (2.20)$$

$$\begin{pmatrix} C_3 \\ D_3 \end{pmatrix} = -\frac{i\nu_c}{k} \begin{pmatrix} D_1 \\ C_1 \end{pmatrix} \quad (2.21)$$

Next, we shall consider symmetric and antisymmetric motion separately, as shown in Figure 2.1. In symmetric motion,  $u$  will be even while  $w$  will be odd, and vice versa in antisymmetric motion. So we shall consider symmetric motion and set  $B_1 = D_1 = 0$ . This gives us

$$u = A_1 \cosh \nu_s z + C_1 \cosh \nu_c z \quad (2.22)$$

$$v = A_2 \cosh \nu_s z + B_2 \sinh \nu_s z \quad (2.23)$$

$$w = -\frac{ikA_1}{\nu_s} \sinh \nu_s z - \frac{i\nu_c C_1}{k} \sinh \nu_c z \quad (2.24)$$

For symmetric motion forced by pressures  $p_0 e^{ikx} e^{-i\omega t}$  we have  $\sigma_{xz} = 0$ ,  $\sigma_{yz} = 0$  and  $\sigma_{zz} = -p_0 e^{ikx} e^{-i\omega t}$  at  $z = \pm H$ . Given the information in equation (2.5), the condition reduces to

$$A_1 \frac{(k^2 + \nu_s^2)}{\nu_s} \sinh \nu_s H + 2\nu_c C_1 \sinh \nu_c H = 0 \quad (2.25)$$

$$A_2 = B_2 = 0 \quad (2.26)$$

$$-2A_1 \cosh \nu_s H + \left( \frac{k_s^2}{k^2} - 2 \right) C_1 \cosh \nu_c H = \frac{ip_0}{\mu k} \quad (2.27)$$

We can now solve the linear system in equations (2.25) and (2.27) to obtain  $A_1$  and  $C_1$ . This allows us to find  $w(H) e^{ikx} e^{-i\omega t}$ , the normal displacement of the upper surface. We eventually find

$$w(H) e^{ikx} e^{-i\omega t} = \frac{p_0}{\omega^2 \rho_p S(k)} e^{ikx} e^{-i\omega t} \quad (2.28)$$

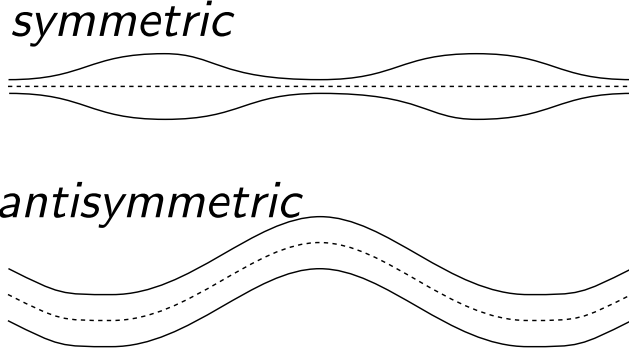


Figure 2.1: Symmetric and antisymmetric modes of motion, exaggerated for clarity

where

$$S(k) = \frac{(k^2 + \nu_s^2)^2}{\nu_c k_s^4} \coth \nu_c H - \frac{4k^2 \nu_s^2}{\nu_s k_s^4} \coth \nu_s H \quad . \quad (2.29)$$

Note here that  $S(k)$  is *even* in  $\nu_c$  and  $\nu_s$ . This means that the choice of sign for these propagation parameters is irrelevant.

In this symmetric motion, the pressure acting on the plate from either side is given by  $p_0 e^{ikx - i\omega t}$ , and the  $z$ -velocities of the upper and lower surfaces of the plate are  $\pm \dot{w}_0 e^{ikx} e^{-i\omega t}$  respectively, where  $\dot{w}_0 = -i\omega w(H)$ . Then the *impedance* of this motion, a function of  $\omega$ ,  $k$  and the properties of the material, is defined by Junger and Feit [8] to be

$$z_s = \frac{p_0}{(-\dot{w}_0)} \quad . \quad (2.30)$$

But from equation (2.28) we find that

$$\dot{w}_0 = -\frac{ip_0}{\omega \rho_p S(k)} \quad . \quad (2.31)$$

Therefore,

$$z_s = -i\omega \rho_p S(k) \quad . \quad (2.32)$$

For a freely propagating symmetric mode, we have propagation with no applied pressure, so the impedance must be zero, or  $S(k) = 0$ . This is the dispersion relation for the symmetric mode.

Now we shall consider antisymmetric motion. The pressure acting on the upper side of the plate will be  $p_0 e^{ikx - i\omega t}$  while the pressure acting on the lower side will be  $-p_0 e^{ikx - i\omega t}$ . In a similar way, the  $z$ -velocity of both surfaces will be  $\dot{w}_0 e^{ikx - i\omega t}$ , for  $\dot{w}_0$  as defined earlier. Then the impedance for this motion will be

$$z_a = \frac{p_0}{(-\dot{w}_0)} \quad . \quad (2.33)$$

This can be shown to be

$$z_a = -i\omega \rho_p A(k) \quad (2.34)$$

where

$$A(k) = \frac{(k^2 + \nu_s^2)^2}{\nu_c k_s^4} \tanh \nu_c H - \frac{4k^2 \nu_s^2}{\nu_s k_s^4} \tanh \nu_s H \quad (2.35)$$

which, like  $S(k)$ , is even in both  $\nu_c$  and  $\nu_s$ . Therefore we find the dispersion relation for free antisymmetric modes to be given by  $A(k) = 0$ .

We shall discuss impedances further in section 2.3.

## 2.2 Motion with Fluid Loading

With the presence of fluid below the thick plate — that is, for  $z < -H$  — we will now excite the top surface of the plate with an excitation  $P e^{ikx} e^{-i\omega t}$  where  $P$  is a constant, as in Figure 2.2. This fluid will have density  $\rho_0$  and sound speed  $c_0$ . Assume also that the pressure in the fluid below the plate is given by  $p(x, z, t) = p(z) e^{ikx} e^{-i\omega t}$ . Of course, there is fluid above the plate in practice (that

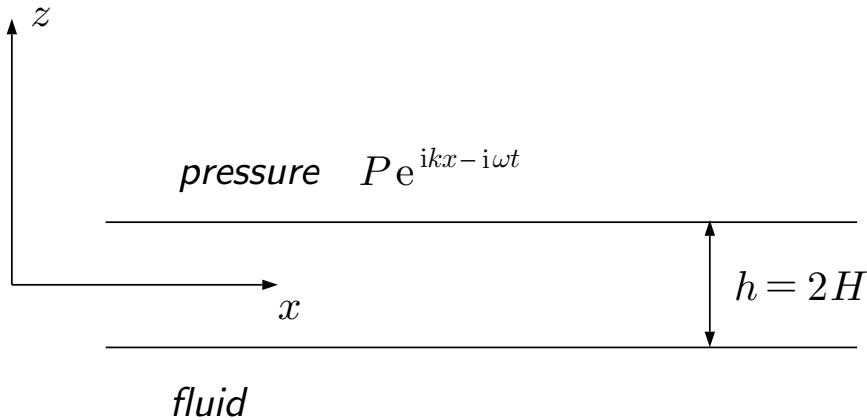


Figure 2.2: The infinite thick plate with fluid loading

is, for  $z > H$ ), but here we are only looking at the interaction of a *prescribed* pressure on  $z = H$  with the plate and fluid below.

Then the boundary conditions for the stresses in the plate become  $\sigma_{xz} = \sigma_{yz} = 0$  at  $z = \pm H$ , and

$$\sigma_{zz} \Big|_{z=H} = -P e^{ikx} e^{-i\omega t} \quad (2.36)$$

$$\sigma_{zz} \Big|_{z=-H} = -p(-H) e^{ikx} e^{-i\omega t} \quad . \quad (2.37)$$

As shown previously,  $u$ ,  $v$  and  $w$  are given by

$$u = A_1 \cosh \nu_s z + B_1 \sinh \nu_s z + C_1 \cosh \nu_c z + D_1 \sinh \nu_c z \quad (2.38)$$

$$v = A_2 \cosh \nu_s z + B_2 \sinh \nu_s z \quad (2.39)$$

$$w = -\frac{ikB_1}{\nu_s} \cosh \nu_s z - \frac{ikA_1}{\nu_s} \sinh \nu_s z - \frac{i\nu_c D_1}{k} \cosh \nu_c z - \frac{i\nu_c C_1}{k} \sinh \nu_c z \quad . \quad (2.40)$$

The conditions  $\sigma_{yz}|_{z=\pm H} = 0$  give  $A_2 = B_2 = 0$ , so that  $v(z) = 0$ . The other four conditions give us a linear system for the four remaining constants, which can be written as

$$\left( \begin{array}{c|c} \mathbf{S} & \mathbf{A} \\ \hline \mathbf{S} & -\mathbf{A} \end{array} \right) \begin{pmatrix} A_1 \\ C_1 \\ B_1 \\ D_1 \end{pmatrix} = \frac{i}{kc_s^2 \rho_p} \begin{pmatrix} 0 \\ P \\ 0 \\ p(-H) \end{pmatrix} \quad (2.41)$$

where

$$\mathbf{S} = \begin{pmatrix} \left( \frac{k^2 + \nu_s^2}{\nu_s} \right) \sinh \nu_s H & 2\nu_c \sinh \nu_c H \\ -2 \cosh \nu_s H & -\left( \frac{k^2 + \nu_s^2}{k^2} \right) \cosh \nu_c H \end{pmatrix} \quad (2.42)$$

$$\mathbf{A} = \begin{pmatrix} \left( \frac{k^2 + \nu_s^2}{\nu_s} \right) \cosh \nu_s H & 2\nu_c \cosh \nu_c H \\ -2 \sinh \nu_s H & -\left( \frac{k^2 + \nu_s^2}{k^2} \right) \sinh \nu_c H \end{pmatrix} \quad (2.43)$$

so that

$$S(k) = \frac{-k^2 \nu_s}{\sinh(\nu_s H) \sinh(\nu_c H) \nu_c k_s^4} \det \mathbf{S} \quad (2.44)$$

$$A(k) = \frac{-k^2 \nu_s}{\cosh(\nu_s H) \cosh(\nu_c H) \nu_c k_s^4} \det \mathbf{A} \quad . \quad (2.45)$$

We can thus find expressions for each of  $A_1$ ,  $B_1$ ,  $C_1$  and  $D_1$ .

In the water,  $z < -H$ , the pressure is given by  $p(x, z, t) = p(z)e^{ikx}e^{-i\omega t}$ . The fluid density is given by  $\rho_0$  and the speed of sound is  $c_0$ . We shall also use the fluid acoustic wavenumber  $k_0 = \omega/c_0$ .

At the fluid-solid interface, the normal component of the solid acceleration must match the normal component of the fluid acceleration. This is encapsulated in Euler's equation (as given by Junger and Feit [8]),

$$\frac{\partial p}{\partial z} = -\rho_0 \frac{\partial^2 u_z}{\partial t^2} \quad \text{at } z = -H. \quad (2.46)$$

But  $u_z = w(z)e^{ikx}e^{-i\omega t}$  and  $p$  is given above, so

$$p'(-H) = \rho_0 \omega^2 w(-H) \quad (2.47)$$

which can be simplified to

$$p'(-H) = \frac{\rho_0}{2\rho_p} \left( \frac{P - p(-H)}{A(k)} - \frac{P + p(-H)}{S(k)} \right) \quad (2.48)$$

with the help of equations (2.44) and (2.45). However, the pressure in the fluid satisfies the wave equation,

$$\nabla^2 p - \frac{1}{c_0^2} \frac{\partial^2 p}{\partial t^2} = 0 \quad (2.49)$$

or

$$\left(\frac{\partial^2}{\partial z^2} - (k^2 - k_0^2)\right)p(z) = 0 \quad . \quad (2.50)$$

On defining  $\nu_0 = \sqrt{k^2 - k_0^2}$  to be the fluid acoustic-wave normal propagation parameter, we have a general solution to the pressure given by

$$p(z) = A_+ e^{\nu_0 z} + A_- e^{-\nu_0 z} \quad (2.51)$$

where  $A_+$  and  $A_-$  are constants. If  $\nu_0$  is real, then  $p$  must decrease as  $z \rightarrow -\infty$ . Thus we must have  $A_- = 0$ . However, if  $\nu_0$  is imaginary, we must have waves travelling downwards, that is  $p \propto e^{-i\gamma z - i\omega t}$  for some  $\gamma > 0$  (assuming  $\omega > 0$ , which is the case here). So for imaginary  $\nu_0$  we must have  $A_+ = 0$ . We therefore assume that  $p(z) = A e^{\nu_0 z}$  while imposing the constraint that if  $\nu_0$  is real, we take the positive square root, and if  $\nu_0$  is imaginary we take it to have negative imaginary part.

We now substitute this into equation (2.48) to get, eventually,

$$p(x, z, t) = \frac{\left(\frac{\rho_0}{\nu_0 \rho_p}\right) P(S(k) - A(k))}{2S(k)A(k) + \left(\frac{\rho_0}{\nu_0 \rho_p}\right) (S(k) + A(k))} e^{\nu_0(H+z)} e^{ikx} e^{-i\omega t} \quad . \quad (2.52)$$

This is the form given in the original analysis of the problem by Thales [18].

Note that when  $\nu_0$  is real, or  $k > k_0$ , the pressure attenuates as we move further into the fluid. In this instance the excitation is subsonic with respect to the water, since  $\omega/k < c_0$ . However, when  $k < k_0$ ,  $\nu_0$  is imaginary, waves radiate into the fluid, and we have supersonic excitation.

The value of the sound level in decibels — the sound pressure level (SPL) — is given (see Junger and Feit [8] for example) by the formula

$$\text{SPL} = 20 \log_{10} \left( \frac{\langle p \rangle}{p_0} \right) \quad (2.53)$$

where  $\langle p \rangle$  is the root mean square of  $p$  and  $p_0$  is a reference pressure. Here we choose  $p_0$  to be the root mean square of the incident pressure. Applying this to equation (2.52) with the values given in the introduction and  $z = -H$  (in other words, measuring the pressure on the lower surface) gives us the graph shown in Figure A.2.

The values in the introduction also give us the value of the longitudinal wavenumber  $k_1$ , which satisfies  $S(k_1) = 0$ , and the bending wavenumber  $k_2$ , which satisfies  $A(k_2) = 0$ . We find that  $k_1 = 13.04 \text{ m}^{-1}$  and  $k_2 = 35.89 \text{ m}^{-1}$ . Additionally the acoustic wavenumber is  $k_0 = 20.94 \text{ m}^{-1}$ . We can therefore identify the cause of each of the peaks in the graph. The first is due to the longitudinal vibration in the plate, the second due to the transition between supersonic and subsonic excitation at  $k = k_0$ , and the third due to the transverse vibration in the plate. It is noticeable, however, that the peak due to the transverse vibration of the thick plate is at a wavenumber higher than  $k_2$ . The reason for this is that in vacuo, excitation at the wavenumber  $35.89 \text{ m}^{-1}$  gives a natural frequency of

5 kHz to the plate. However, if we consider motion with fluid below the plate, the kinetic energy of the motion will have increased while the potential energy remains the same. This increased kinetic energy leads to a lower natural frequency at the given wavenumber  $k_2 = 35.89 \text{ m}^{-1}$ , as shown by Rayleigh [16]. So, for resonance at the given frequency 5 kHz, we must have a greater wavenumber than  $k_2$ .

## 2.3 Impedances

We can also solve the problem above by the impedance method. We have already defined the impedances for symmetric motion, equation (2.30), and for antisymmetric motion, equation (2.33), and have shown that they are given respectively by

$$z_s = -i\omega\rho_p S(k) \quad (2.54)$$

$$z_a = -i\omega\rho_p A(k) \quad (2.55)$$

Now, consider the interface between the plate and a region of fluid below it. If the pressure in the fluid on the plate is given by  $p_0 e^{ikx-i\omega t}$  and the  $z$ -velocity of the plate surface is given by  $\dot{w}_0 e^{ikx-i\omega t}$ , then the fluid impedance will be given by

$$z_f = \frac{p_0}{(-\dot{w}_0)} \quad (2.56)$$

To calculate this quantity, first we use the wave equation (2.49) to show that the pressure in the fluid is given by  $p_0 e^{ikx-i\omega t+\nu_0 z}$ , using the same convention on the sign of  $\nu_0$ . Then, substituting the pressure and the velocity of the plate into Euler's equation (2.46) gives us

$$z_f = \frac{p_0}{(-\dot{w}_0)} = -\frac{i\omega\rho_0}{\nu_0} = -i\omega\rho_p \frac{\rho_0}{\rho_p\nu_0} \quad (2.57)$$

If we now consider the situation of the thick plate with water beneath it, and excited on its upper surface, we can prescribe the pressure above to be  $P e^{ikx-i\omega t}$  and let the pressure below be  $p_l e^{ikx-i\omega t}$ ; in addition let the velocities (acting in the positive  $z$ -direction) of the upper and lower surfaces be given respectively by  $\dot{w}_0 e^{ikx-i\omega t}$  and  $\dot{w}_l e^{ikx-i\omega t}$ .

Now, we can split up this motion into symmetric and antisymmetric motions. In the symmetric motion we have pressure on either surface to be  $\frac{1}{2}(P+p_l)$  and their  $z$ -velocities to be  $\pm\frac{1}{2}(\dot{w}_0 - \dot{w}_l)$ . This leads to

$$\frac{1}{2}(P+p_l) = \frac{z_s}{2}(\dot{w}_l - \dot{w}_0) \quad (2.58)$$

from equation (2.30). Conversely, the antisymmetric motion is characterised by pressures on the upper and lower surfaces of  $\pm\frac{1}{2}(P-p_l)$  respectively, and each surface having a  $z$ -velocity of  $\frac{1}{2}(\dot{w}_0 + \dot{w}_l)$ .

This leads to

$$\frac{1}{2}(p_l - P) = \frac{z_a}{2}(\dot{w}_l + \dot{w}_0) \quad (2.59)$$

from equation (2.33). Finally, from equation (2.56) we get

$$p_l = -z_f \dot{w}_l \quad . \quad (2.60)$$

On elimination of  $\dot{w}_0$  and  $\dot{w}_l$  we get

$$p_l = \frac{z_f P(z_s - z_a)}{2z_a z_s + z_f(z_a + z_s)} \quad . \quad (2.61)$$

Now, we substitute our calculated values of  $z_s$ ,  $z_a$  and  $z_f$  to find that

$$p_l = \frac{\left(\frac{\rho_0}{\nu_0 \rho_p}\right) P(S(k) - A(k))}{2S(k)A(k) + \left(\frac{\rho_0}{\nu_0 \rho_p}\right) (S(k) + A(k))} \quad . \quad (2.62)$$

Comparing this with equation (2.52) (remembering that  $p_l$  is the amplitude of the pressure on the lower surface), we find that we have replicated the previous result. Thus  $S(k)$ ,  $A(k)$  and  $\frac{\rho_0}{\nu_0 \rho_p}$  correspond to scaled impedances, the scaling factor being  $-i\omega\rho_p$ .

## 2.4 Thin Plate Approximation

For a plate which is deemed thin, that is, for which the thickness is small compared to the wavelength of waves under consideration, the equation for  $w$ , the transverse displacement of the mid-surface of the plate, is

$$\frac{Eh^3}{12(1-\nu^2)} \nabla^4 w + \rho_p h \frac{\partial^2 w}{\partial t^2} = F \quad (2.63)$$

where  $E$  is the Young's modulus and  $\nu$  the Poisson ratio of the material, and  $F$  is the total external normal force per unit area on the plate. We can express  $E$  and  $\nu$  in terms of the Lamé constants by (see Love [12])

$$E = \frac{\mu(3\lambda + 2\mu)}{\lambda + \mu} \quad (2.64)$$

and

$$\nu = \frac{\lambda}{2(\lambda + \mu)} \quad . \quad (2.65)$$

In this case, we let

$$F = -p|_{\text{top}} + p|_{\text{bottom}} \quad (2.66)$$

where  $p|_{\text{top}} = P e^{ikx - i\omega t}$  in this instance.

Assuming a displacement of the form  $w = w_0 e^{ikx - i\omega t}$  and applying Euler's equation (2.46) at  $z = 0$  (since the plate is assumed to be infinitesimally thin) finally gets us a pressure on the underside of the plate given by

$$p_l = P \left( 1 + \frac{\rho_p h \nu_0}{\rho_0} - \frac{E h^3 k^4 \nu_0}{12(1-\nu^2) \rho_0 \omega^2} \right)^{-1} \quad . \quad (2.67)$$

The graph of this pressure, in decibels, can be seen in Figure A.1.

We see an effect due to transverse bending waves, which have a wavenumber  $k = 29.3 \text{ m}^{-1}$  in vacuo, but the peak occurs at a higher wavenumber for the same reason as for the thick plate. We also see the small peak representing the transition between supersonic and subsonic excitation that we saw for thick plate motion. No effect is seen that could be attributed to longitudinal motion in the thin plate, because we have only considered transverse motion of the plate in this case.

The main reason that the thin plate approximation is invalid in our case is that it is valid only where  $kH \ll 1$ . In our case, though, taking a representative value for  $k$  — for example, the longitudinal wavenumber 13 — gives us  $kH = 0.65$ , which does not satisfy the assumption.

Thin plate theory is useful, however, for a discussion of the nature of the fluid loading in this case. Crighton and Innes [6] define fluid loading in the following way. The *intrinsic fluid loading parameter* is defined by

$$\varepsilon = \frac{\rho_0}{\rho_p} \sqrt{\frac{E}{12\rho_p c_0^2(1-\nu^2)}} \quad (2.68)$$

which gives  $\varepsilon \approx 0.289$  using the same values used up to now. The second parameter used is the Mach number  $M$ , defined by  $M = k_0/k_b$  where

$$k_b = \left( \frac{12(1-\nu^2)\rho_p\omega^2}{Eh^2} \right)^{1/4} \quad (2.69)$$

is the thin plate bending wavenumber. This gives us  $M \approx 0.698$  in our case. Crighton and Innes state that if  $M = O(1)$  then we have light fluid loading; if  $M = O(\varepsilon)$  then the fluid loading is significant; and if  $M \ll \varepsilon$  then we have heavy fluid loading. We thus deduce that the fluid loading can reasonably be treated as light in this case.

## 2.5 Thick Plate with a Rigid Boundary

We shall now consider the situation depicted in Figure 2.3, where the upper surface, as before, is excited by a pressure  $P e^{ikx} e^{-i\omega t}$ . The hydrophones and the hull are much stiffer than the GRP

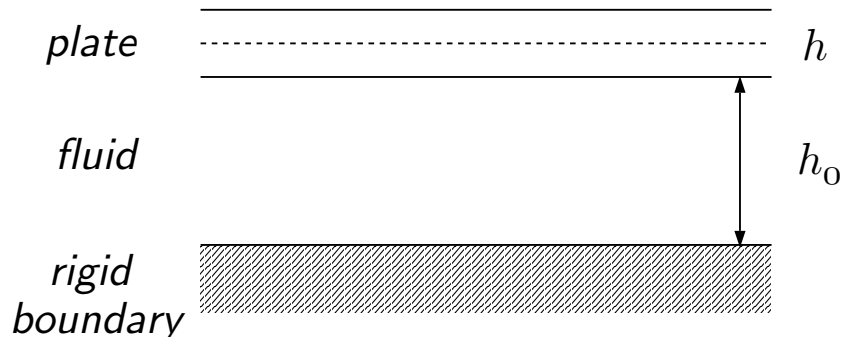


Figure 2.3: Thick plate with a rigid boundary

sonar dome, so we treat them as rigid. From previous work, we know that

$$p(z) = A_+ e^{\nu_0 z} + A_- e^{-\nu_0 z} \quad (2.70)$$

from equation (2.51), and additionally that Euler's equation (2.46) holds at each boundary. Therefore, the pressure  $p$  satisfies

$$p'(-H) = \frac{\rho_0}{2\rho_p} \left( \frac{P - p(-H)}{A(k)} - \frac{P + p(-H)}{S(k)} \right) \quad (2.71)$$

$$p'(-(H + h_0)) = 0 \quad (2.72)$$

Equation (2.72) gives

$$p(z) = A_+ (e^{\nu_0 z} + e^{-2\nu_0(H+h_0)-\nu_0 z}) \quad , \quad (2.73)$$

which can be substituted into equation (2.71) to give, finally,

$$p(x, z, t) = \frac{P \frac{\rho_0}{\rho_p \nu_0} (S(k) - A(k)) \cosh(\nu_0(H + H_0 + z))}{2A(k)S(k) \sinh(\nu_0 h_0) + \frac{\rho_0}{\rho_p \nu_0} (S(k) + A(k)) \cosh(\nu_0 h_0)} e^{ikx} e^{-i\omega t} \quad . \quad (2.74)$$

We can now compare the pressure at a distance  $h_0$  from the plate, with and without the rigid boundary. The results are shown in Figure A.4. We see clearly that the peak due to compressive effects in the plate is much more pronounced with the rigid boundary than without. However we also see two other peaks which are due to resonances of this composite waveguide.

For comparison, the pressure in water with a rigid boundary at a distance  $h_0$  from a thin plate excited in the same way is given by

$$p(x, z, t) = \frac{P \cosh(\nu_0(z - h_0)) e^{-i\omega t}}{\cosh(\nu_0 h_0) - \left( \frac{Eh^3 k^4}{12(1 - \nu^2)} - \rho_p h \omega^2 \right) \frac{\nu_0}{\rho_0 \omega^2} \sinh(\nu_0 h_0)} \quad (2.75)$$

using similar methods. The graph of the pressure at a distance  $h_0$  from the plate is shown in Figure A.3.

## 2.6 Discussion

The results displayed in Figure A.2 do not sufficiently explain the effects seen in the experimental measurements seen by the sonar array — the effect due to the compressive waves in the plate is smaller than we had hoped for. Additionally, while we may expect the effect due to bending waves to be significant, this is not so because this effect occurs at a subsonic wavenumber so the disturbance is well attenuated by the time it reaches the hydrophones in the sonar array. The graph in Figure A.4, however, does display a stronger response to excitation at a wavenumber near plate compressive wavenumbers. Interestingly, it also displays several peaks at nearby wavenumbers, which were not expected. These are not caused by compressive effects, because they also appear in the same situation

when a thin plate is considered, in Figure A.3. We must conclude, therefore, that they are a product of the rigid boundary placed behind the plate — that is, that they are due to a resonance effect in the fluid. These effects have not previously been considered in Thales' analysis of these domes and arrays, but clearly should be taken into account.

## Chapter 3

# Analysis of an Infinite Cylindrical Shell

In this chapter we will investigate the situation of an infinitely long thin cylindrical shell, filled with water and investigate the pressure in the interior when the exterior is excited by a pressure that varies sinusoidally in the circumferential direction. Following this we shall introduce a rigid cylinder to the interior and investigate the pressure on this cylinder's surface, comparing it to the earlier situation.

Secondly, we shall derive the equations of a thick cylindrical shell, from the equations of linear elasticity. We will then apply these to the problems described above.

### 3.1 Thin Cylindrical Shell

We consider a cylindrical shell of thickness  $h$  which is infinitely long in the  $z$ -direction, as shown in Figure 3.1. We further assume the radius of the middle surface of the cylinder to be  $R$ , and  $h \ll R$ .

Now we let  $u_r$ ,  $u_\theta$  and  $u_z$  be the components of displacement of the middle surface of the shell in the  $r$ ,  $\theta$  and  $z$  directions respectively. The equations of free motion — that is, with no applied forces — are given by Junger and Feit [8] and Leissa [10] by

$$\mathcal{L} \begin{pmatrix} u_r \\ u_\theta \\ u_z \end{pmatrix} = \begin{pmatrix} 0 \\ 0 \\ 0 \end{pmatrix} \quad (3.1)$$

where  $\mathcal{L}$  is a matrix differential operator. There are several different forms of  $\mathcal{L}$  in the literature, depending on how systematically the asymptotics of the limit  $h/R \rightarrow 0$  are treated, and which terms are neglected on physical grounds in particular applications. Leissa [10] reviews the different forms. One of the most generally applicable forms for  $\mathcal{L}$  is the form given by Arnold-Warburton (or Goldenveizer-Novozhilov) theory, where the operator is expressed by

$$\mathcal{L} = \mathcal{L}_{\text{DM}} + \kappa \mathcal{L}_{\text{AW}} \quad (3.2)$$

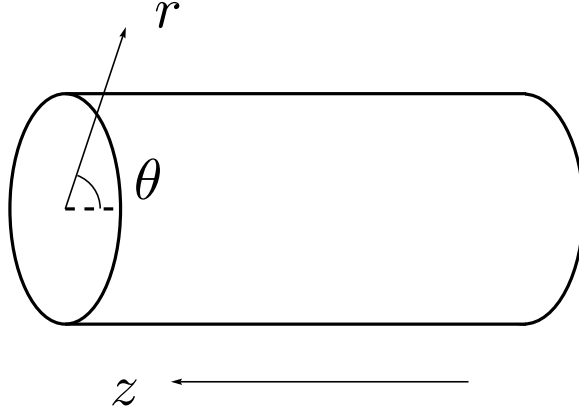


Figure 3.1: Cylindrical coordinates

where  $\kappa$  is the nondimensional parameter given by

$$\kappa = \frac{h^2}{12R^2} . \quad (3.3)$$

Here,  $\mathcal{L}_{\text{DM}}$  is the operator from the Donnell-Mushtari theory of shells, and  $\mathcal{L}_{\text{AW}}$  is a modifying operator. In this scheme the operators are given by

$$\mathcal{L}_{\text{DM}} = \begin{pmatrix} \frac{1}{R^2} + R^2\kappa\nabla^4 & \frac{1}{R^2} \frac{\partial}{\partial\theta} & \frac{\nu}{R} \frac{\partial}{\partial z} \\ + \frac{\rho_p(1-\nu^2)}{E} \frac{\partial^2}{\partial t^2} & & \\ \frac{1}{R^2} \frac{\partial}{\partial\theta} & \frac{1-\nu}{2} \frac{\partial^2}{\partial z^2} + \frac{1}{R^2} \frac{\partial^2}{\partial z \partial\theta} & \frac{1+\nu}{2R} \frac{\partial^2}{\partial z \partial\theta} \\ - \frac{\rho_p(1-\nu^2)}{E} \frac{\partial^2}{\partial t^2} & & \\ \frac{\nu}{R} \frac{\partial}{\partial z} & \frac{1+\nu}{2R} \frac{\partial^2}{\partial z \partial\theta} & \frac{\partial^2}{\partial z^2} + \frac{1-\nu}{2R^2} \frac{\partial^2}{\partial\theta^2} \\ - \frac{\rho_p(1-\nu^2)}{E} \frac{\partial^2}{\partial t^2} & & \end{pmatrix} \quad (3.4)$$

and

$$\mathcal{L}_{\text{AW}} = \begin{pmatrix} 0 & -(2-\nu) \frac{\partial^3}{\partial z^2 \partial\theta} - \frac{1}{R^2} \frac{\partial^3}{\partial\theta^3} & 0 \\ -(2-\nu) \frac{\partial^3}{\partial z^2 \partial\theta} - \frac{1}{R^2} \frac{\partial^3}{\partial\theta^3} & 2(1-\nu) \frac{\partial^2}{\partial z^2} + \frac{1}{R^2} \frac{\partial^2}{\partial\theta^2} & 0 \\ 0 & 0 & 0 \end{pmatrix} \quad (3.5)$$

where  $E$  is Young's modulus,  $\nu$  is Poisson's ratio — which are expressed in terms of the Lamé moduli  $\lambda$  and  $\mu$  in equations (2.64) and (2.65) — and  $\nabla^4$  is the in-surface biharmonic operator, given by

$$\nabla^4 = \left( \frac{\partial^2}{\partial z^2} + \frac{1}{R^2} \frac{\partial^2}{\partial \theta^2} \right)^2 . \quad (3.6)$$

### 3.1.1 Motion with Fluid Loading

We shall be considering first an infinite cylindrical shell, filled with water, with an applied pressure  $P e^{iks} e^{-i\omega t}$  on its exterior, where  $s = R\theta$  is the circumferential coordinate of the shell. (We should properly have used  $R + h/2$  here instead of  $R$ , but we follow the standard practice in thin shell theory of dropping terms in  $h/R$  from the boundary conditions.) This leads to a constraint on the possible values of  $k$ , because the pressure at  $\theta = 0$  must equal the pressure at  $\theta = 2\pi$ . Therefore, given that the applied pressure is proportional to  $e^{ikR\theta}$ , we must only allow integer values of  $kR$ , or restrict  $k$  to have values  $n/R$  for all integers  $n$ .

In the presence of external forces acting on the cylinder, equation (3.1) is modified to

$$\mathcal{L} \begin{pmatrix} u_r \\ u_\theta \\ u_z \end{pmatrix} = \begin{pmatrix} \frac{(1-\nu^2)F}{Eh} \\ 0 \\ 0 \end{pmatrix} \quad (3.7)$$

where  $F$  is the total force per unit area acting in the radial direction. But if we let the pressure on the inside of the shell be given by  $p_l e^{ikR\theta} e^{-i\omega t}$  (assuming that all variables will be proportional to  $e^{ikR\theta} e^{-i\omega t}$ ) then our equations of motion become

$$(\mathcal{L}_{\text{DM}} + \kappa \mathcal{L}_{\text{AW}}) \begin{pmatrix} u_r \\ u_\theta \\ u_z \end{pmatrix} = \begin{pmatrix} \frac{(1-\nu^2)(p_l - P)}{Eh} \\ 0 \\ 0 \end{pmatrix} e^{ikR\theta} e^{-i\omega t} . \quad (3.8)$$

Now we assume that the displacements  $u_r$ ,  $u_\theta$  and  $u_z$  have no  $z$ -dependence, and write

$$u_r = u e^{ikR\theta - i\omega t} \quad (3.9)$$

$$u_\theta = v e^{ikR\theta - i\omega t} \quad (3.10)$$

$$u_z = w e^{ikR\theta - i\omega t} \quad (3.11)$$

for constants  $u$ ,  $v$  and  $w$ . Then the equations (3.8) become

$$\left( \frac{1}{R^2} + \kappa k^4 R^2 - \frac{\rho_p(1-\nu^2)\omega^2}{E} \right) u + \left( \frac{ik}{R} + i\kappa k^3 R \right) v = \frac{(p_l - P)(1-\nu^2)}{Eh} \quad (3.12)$$

$$\left( \frac{ik}{R} + i\kappa k^3 R \right) u + \left( \frac{\rho_p(1-\nu^2)\omega^2}{E} - (1+\kappa)k^2 \right) v = 0 \quad (3.13)$$

$$\left( \frac{\rho_p(1-\nu^2)\omega^2}{E} - \frac{k^2(1-\nu)}{2} \right) w = 0 . \quad (3.14)$$

Therefore  $w = 0$ , and also,

$$u = (p_l - P)\xi \quad (3.15)$$

where

$$\xi = \frac{\left(\frac{\rho_p(1-\nu^2)\omega^2}{E} - (1+\kappa)k^2\right) \frac{1-\nu^2}{Eh}}{\left(\frac{k}{R} + \kappa k^3 R\right)^2 + \left(\frac{\rho_p(1-\nu^2)\omega^2}{E} - (1+\kappa)k^2\right) \left(\frac{1}{R^2} + \kappa k^4 R^2 - \frac{\rho_p(1-\nu^2)\omega^2}{E}\right)} \quad (3.16)$$

is a constant. We will not need to use  $\nu$  in any further calculations.

Next we will consider the pressure  $p(r, \theta, t)$  in the fluid surrounded by the cylindrical shell (we again assume no  $z$ -dependence). This pressure satisfies the wave equation,

$$\nabla^2 p - \frac{1}{c_0^2} \frac{\partial^2 p}{\partial t^2} = 0 \quad (3.17)$$

for  $r < R$ . We let  $p = p(r, \theta)e^{-i\omega t}$  to obtain the Helmholtz equation, as before:

$$\nabla^2 p + k_0^2 p = 0 \quad . \quad (3.18)$$

In cylindrical polar coordinates, we have (see, for example, Bourne and Kendall [3])

$$\nabla^2 = \frac{\partial^2}{\partial r^2} + \frac{1}{r} \frac{\partial}{\partial r} + \frac{1}{r^2} \frac{\partial^2}{\partial \theta^2} + \frac{\partial^2}{\partial z^2} \quad (3.19)$$

so that

$$\frac{\partial^2 p}{\partial r^2} + \frac{1}{r} \frac{\partial p}{\partial r} + \frac{1}{r^2} \frac{\partial^2 p}{\partial \theta^2} + k_0^2 p = 0 \quad . \quad (3.20)$$

The boundary conditions for this equation are that  $p$  is finite at  $r = 0$  and that  $p = p_l e^{ikR\theta}$  at  $r = R$ .

To solve the equation, we separate variables,

$$p(r, \theta) = A(r)B(\theta) \quad , \quad (3.21)$$

obtaining

$$\frac{r^2 A''(r)}{A(r)} + \frac{r A'(r)}{A(r)} + k_0^2 r^2 = \frac{-B''(\theta)}{B(\theta)} \quad . \quad (3.22)$$

The sides are independent of each other, so we put both equal to a constant, say  $C^2$ . Then, the  $\theta$  equation becomes

$$B''(\theta) + C^2 B(\theta) = 0 \quad (3.23)$$

so that

$$B(\theta) = B_1 e^{iC\theta} + B_2 e^{-iC\theta} \quad . \quad (3.24)$$

But  $p|_{r=R} = p_l e^{ikR\theta}$ , so  $B_2 = 0$  and  $C = kR$ . Then, the  $r$  equation becomes

$$r^2 A''(r) + r A'(r) + (k_0^2 r^2 - k^2 R^2) A(r) = 0 \quad . \quad (3.25)$$

This is Bessel's equation (see Abramowitz and Stegun [1]), and has solutions

$$A(r) = A_1 J_{kR}(k_0 r) + A_2 Y_{kR}(k_0 r) \quad . \quad (3.26)$$

We must have  $A_2 = 0$  to avoid a singularity at  $r = 0$ . This then leaves us with

$$p(r, \theta) = AJ_{kR}(k_0r)e^{ikR\theta} \quad . \quad (3.27)$$

Applying the condition  $p|_{r=R} = p_l e^{ikR\theta}$  gives the pressure in the water to be

$$p(r, \theta, t) = p_l \frac{J_{kR}(k_0r)}{J_{kR}(k_0R)} e^{ikR\theta - i\omega t} \quad . \quad (3.28)$$

In cylindrical polar coordinates, Euler's equation (2.46) takes the form

$$\frac{\partial p}{\partial r} = -\rho_0 \frac{\partial^2 u_r}{\partial t^2} \quad \text{at} \quad r = R. \quad (3.29)$$

We have  $p$  given by equation (3.28), and

$$u_r = (p_l - P)\xi e^{ikR\theta} e^{-i\omega t} \quad (3.30)$$

where  $\xi$  is given by equation (3.16). We substitute this into equation (3.29) to get

$$\frac{p_l k_0 J'_{kR}(k_0R)}{J_{kR}(k_0R)} = \omega^2 \rho_0 \xi (p_l - P) \quad . \quad (3.31)$$

We obtain a value for  $p_l$ ,

$$p_l = \frac{P \rho_0 \omega^2 \xi}{\rho_0 \omega^2 \xi - \frac{k_0 J'_{kR}(k_0R)}{J_{kR}(k_0R)}} \quad . \quad (3.32)$$

To calculate the values of the derivatives of the Bessel functions, we need to use the relations in Abramowitz and Stegun [1]:

$$J'_\nu(z) = J_{\nu-1}(z) - \frac{\nu}{z} J_\nu(z) \quad (3.33)$$

$$Y'_\nu(z) = Y_{\nu-1}(z) - \frac{\nu}{z} Y_\nu(z) \quad , \quad (3.34)$$

but we will choose not to expand the derivatives here.

### 3.1.2 Inclusion of a Rigid Cylinder

Now we will consider the configuration depicted in Figure 3.2, where the cylindrical shell of the previous section has a rigid cylinder in its interior, surrounded by fluid. The exterior is still excited by a pressure  $P e^{ikR\theta} e^{-i\omega t}$ , with the same restriction on the possible values of  $k$ .

From equation (3.26) the pressure in the fluid is given by

$$p = (A_1 J_{kR}(k_0r) + A_2 Y_{kR}(k_0r)) e^{ikR\theta - i\omega t} \quad . \quad (3.35)$$

But  $p|_{r=R} = p_l e^{ikR\theta - i\omega t}$ , so

$$p = p_l \frac{J_{kR}(k_0r) + AY_{kR}(k_0r)}{J_{kR}(k_0R) + AY_{kR}(k_0R)} e^{ikR\theta - i\omega t} \quad (3.36)$$

where  $A = A_2/A_1$  is arbitrary.

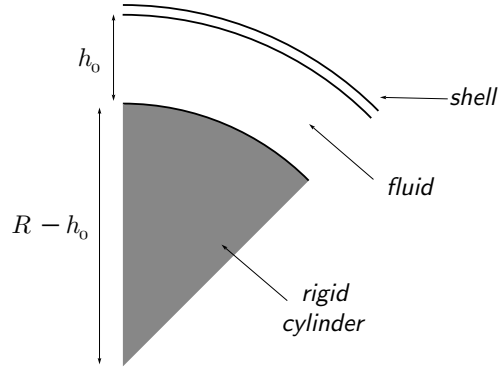


Figure 3.2: Cylindrical shell with rigid cylinder

The boundary conditions for this problem come from applying Euler's equation at  $r = R$  and  $r = R - h_0$ :

$$\left. \frac{\partial p}{\partial r} \right|_{r=R-h_0} = 0 \quad (3.37)$$

$$\left. \frac{\partial p}{\partial r} \right|_{r=R} = -\rho_0 \frac{\partial^2 u_r}{\partial t^2} \quad (3.38)$$

Equation (3.37) gives us

$$A = \frac{-J'_{kR}(k_0(R-h_0))}{Y'_{kR}(k_0(R-h_0))} \quad (3.39)$$

using equations (3.33) and (3.34). At the shell, equation (3.30) is still valid; substituting this, together with the expression for the pressure, into equation (3.38) gives

$$k_0 p_l \frac{J'_{kR}(k_0 R) + AY'_{kR}(k_0 R)}{J_{kR}(k_0 R) + AY_{kR}(k_0 R)} = \rho_0 \omega^2 \xi (p_l - P) \quad (3.40)$$

so that

$$p_l = \frac{P \rho_0 \omega^2 \xi}{\rho_0 \omega^2 \xi - B} \quad (3.41)$$

where

$$B = k_0 \frac{J'_{kR}(k_0 R) + AY'_{kR}(k_0 R)}{J_{kR}(k_0 R) + AY_{kR}(k_0 R)} \quad (3.42)$$

and  $\xi$ ,  $A$  are given in equations (3.16) and (3.39) respectively. The pressure in the fluid is then given by equation (3.36).

## 3.2 Infinite Thick Cylindrical Shell

We shall now examine the case of a thick hollow cylinder filled with water, both with and without a rigid cylinder included inside. The method of solution follows closely the work of Gazis [7] and Mirsky [13].

### 3.2.1 Free Motion

According to Love [12], the equations satisfied by the displacements  $u_r$ ,  $u_\theta$  and  $u_z$  in cylindrical polar coordinates are given by

$$\begin{aligned} \rho_p \frac{\partial^2 u_r}{\partial t^2} = & (\lambda + 2\mu) \frac{\partial}{\partial r} \left( \frac{1}{r} \frac{\partial(ru_r)}{\partial r} + \frac{1}{r} \frac{\partial u_\theta}{\partial \theta} + \frac{\partial u_z}{\partial z} \right) \\ & - \frac{\mu}{r} \frac{\partial}{\partial \theta} \left( \frac{1}{r} \frac{\partial(ru_\theta)}{\partial r} - \frac{1}{r} \frac{\partial u_r}{\partial \theta} \right) + \mu \frac{\partial}{\partial z} \left( \frac{\partial u_r}{\partial z} - \frac{\partial u_z}{\partial r} \right) \end{aligned} \quad (3.43)$$

$$\begin{aligned} \rho_p \frac{\partial^2 u_\theta}{\partial t^2} = & (\lambda + 2\mu) \frac{1}{r} \frac{\partial}{\partial \theta} \left( \frac{1}{r} \frac{\partial(ru_r)}{\partial r} + \frac{1}{r} \frac{\partial u_\theta}{\partial \theta} + \frac{\partial u_z}{\partial z} \right) \\ & - \mu \frac{\partial}{\partial z} \left( \frac{1}{r} \frac{\partial u_z}{\partial \theta} - \frac{\partial u_\theta}{\partial z} \right) + \mu \frac{\partial}{\partial r} \left( \frac{1}{r} \frac{\partial(ru_\theta)}{\partial r} - \frac{1}{r} \frac{\partial u_r}{\partial \theta} \right) \end{aligned} \quad (3.44)$$

$$\begin{aligned} \rho_p \frac{\partial u_z}{\partial t^2} = & (\lambda + 2\mu) \frac{\partial}{\partial z} \left( \frac{1}{r} \frac{\partial(ru_r)}{\partial r} + \frac{1}{r} \frac{\partial u_\theta}{\partial \theta} + \frac{\partial u_z}{\partial z} \right) \\ & - \frac{\mu}{r} \frac{\partial}{\partial r} \left( r \frac{\partial u_r}{\partial z} - r \frac{\partial u_z}{\partial r} \right) + \frac{\mu}{r} \frac{\partial}{\partial \theta} \left( \frac{1}{r} \frac{\partial u_z}{\partial \theta} - \frac{\partial u_\theta}{\partial z} \right) \end{aligned} \quad (3.45)$$

and the stress components are given by

$$\sigma_{rr} = \lambda \left( \frac{1}{r} \frac{\partial(ru_r)}{\partial r} + \frac{1}{r} \frac{\partial u_\theta}{\partial \theta} + \frac{\partial u_z}{\partial z} \right) + 2\mu \frac{\partial u_r}{\partial r} \quad (3.46)$$

$$\sigma_{r\theta} = \mu \left( \frac{1}{r} \frac{\partial u_r}{\partial \theta} + r \frac{\partial}{\partial r} \left( \frac{u_\theta}{r} \right) \right) \quad (3.47)$$

$$\sigma_{rz} = \mu \left( \frac{\partial u_r}{\partial z} + \frac{\partial u_z}{\partial r} \right) . \quad (3.48)$$

Following the method of Mirsky [13], we substitute

$$u_r = \left( \frac{\partial \phi}{\partial r} + \frac{1}{r} \frac{\partial \psi}{\partial \theta} \right) e^{i\gamma z} e^{-i\omega t} \quad (3.49)$$

$$u_\theta = \left( \frac{1}{r} \frac{\partial \phi}{\partial \theta} - \frac{\partial \psi}{\partial r} \right) e^{i\gamma z} e^{-i\omega t} \quad (3.50)$$

$$u_z = im\phi e^{i\gamma z} e^{-i\omega t} \quad (3.51)$$

into equations (3.43)–(3.45), where  $\gamma$  is the axial wavenumber,  $m$  is a constant to be evaluated later, and  $\phi(r, \theta)$ ,  $\psi(r, \theta)$  are *displacement potentials*. We obtain the following relations:

$$\begin{aligned} \frac{\partial}{\partial r} \left[ (\lambda + 2\mu) \left( \frac{\partial^2}{\partial r^2} + \frac{1}{r} \frac{\partial}{\partial r} + \frac{1}{r^2} \frac{\partial^2}{\partial \theta^2} \right) \phi + (\rho_p \omega^2 - \mu \gamma^2 - m\gamma(\lambda + \mu)) \phi \right] \\ + \frac{1}{r} \frac{\partial}{\partial \theta} \left[ \mu \left( \frac{\partial^2}{\partial r^2} + \frac{1}{r} \frac{\partial}{\partial r} + \frac{1}{r^2} \frac{\partial^2}{\partial \theta^2} \right) \psi + (\rho_p \omega^2 - \mu \gamma^2) \psi \right] = 0 \end{aligned} \quad (3.52)$$

$$\begin{aligned} \frac{1}{r} \frac{\partial}{\partial \theta} \left[ (\lambda + 2\mu) \left( \frac{\partial^2}{\partial r^2} + \frac{1}{r} \frac{\partial}{\partial r} + \frac{1}{r^2} \frac{\partial^2}{\partial \theta^2} \right) \phi + (\rho_p \omega^2 - \mu \gamma^2 - m\gamma(\lambda + \mu)) \phi \right] \\ - \frac{\partial}{\partial r} \left[ \mu \left( \frac{\partial^2}{\partial r^2} + \frac{1}{r} \frac{\partial}{\partial r} + \frac{1}{r^2} \frac{\partial^2}{\partial \theta^2} \right) \psi + (\rho_p \omega^2 - \mu \gamma^2) \psi \right] = 0 \end{aligned} \quad (3.53)$$

$$((\lambda + \mu)\gamma + \mu m) \left( \frac{\partial^2}{\partial r^2} + \frac{1}{r} \frac{\partial}{\partial r} + \frac{1}{r^2} \frac{\partial^2}{\partial \theta^2} \right) \phi + (\rho_p \omega^2 - \gamma^2(\lambda + 2\mu)) m \phi = 0 \quad (3.54)$$

Equations (3.52) and (3.53) are satisfied if the following differential equations for  $\phi$  and  $\psi$  hold:

$$(\lambda + 2\mu) \left( \frac{\partial^2}{\partial r^2} + \frac{1}{r} \frac{\partial}{\partial r} + \frac{1}{r^2} \frac{\partial^2}{\partial \theta^2} \right) \phi + (\rho_p \omega^2 - \mu \gamma^2 - m \gamma (\lambda + \mu)) \phi = 0 \quad (3.55)$$

$$\mu \left( \frac{\partial^2}{\partial r^2} + \frac{1}{r} \frac{\partial}{\partial r} + \frac{1}{r^2} \frac{\partial^2}{\partial \theta^2} \right) \psi + (\rho_p \omega^2 - \mu \gamma^2) \psi = 0 \quad (3.56)$$

However, equations (3.55) and (3.54) need to be consistent, and this requirement is ensured by choosing  $m$  to satisfy

$$\frac{m(\rho_p \omega^2 - \gamma^2(\lambda + 2\mu))}{(\lambda + \mu)\gamma + \mu m} = \frac{\rho_p \omega^2 - \gamma^2 \mu - \gamma m(\lambda + \mu)}{\lambda + 2\mu} \quad (3.57)$$

We let both sides of this equation to be equal to  $l^2$  and eliminate  $m$  to obtain a quadratic equation for  $l^2$ ,

$$\mu(\lambda + 2\mu)l^4 - ((\lambda + 3\mu)\rho_p \omega^2 - 2\gamma^2 \mu(\lambda + 2\mu))l^2 + (\rho_p \omega^2 - \gamma^2 \mu)(\rho_p \omega^2 - \gamma^2(\lambda + 2\mu)) = 0 \quad (3.58)$$

with

$$m = \frac{-l^2(\lambda + 2\mu) + \rho_p \omega^2 - \gamma^2 \mu}{\gamma(\lambda + \mu)} \quad (3.59)$$

Equation (3.58) can be factorised to give solutions  $l_1^2$  and  $l_2^2$ :

$$l_1^2 = \frac{\rho_p \omega^2}{\lambda + 2\mu} - \gamma^2 = k_c^2 - \gamma^2 \quad (3.60)$$

$$l_2^2 = \frac{\rho_p \omega^2}{\mu} - \gamma^2 = k_s^2 - \gamma^2 \quad (3.61)$$

The corresponding values of  $m$  are given, by equation (3.59), to be

$$m_1 = \gamma \quad (3.62)$$

$$m_2 = \frac{-l_2^2}{\gamma} \quad (3.63)$$

Let  $\phi_1, \phi_2$  be the functions corresponding to those roots, so that we have three equations for the displacement potentials:

$$\nabla^2 \phi_1 + l_1^2 \phi_1 = 0 \quad (3.64)$$

$$\nabla^2 \phi_2 + l_2^2 \phi_2 = 0 \quad (3.65)$$

$$\nabla^2 \psi + q^2 \psi = 0 \quad (3.66)$$

where

$$q^2 = \frac{\rho_p \omega^2}{\mu} - \gamma^2 = l_2^2 \quad (3.67)$$

and

$$\nabla^2 = \frac{\partial^2}{\partial r^2} + \frac{1}{r} \frac{\partial}{\partial r} + \frac{1}{r^2} \frac{\partial^2}{\partial \theta^2} \quad (3.68)$$

Now we shall solve these equations. First we will assume that  $\psi$  has the form

$$\psi(r, \theta) = f(r)e^{in\theta} \quad (3.69)$$

where  $n$  is an integer that will be related later to the wavenumber of the excitation applied to the cylinder. Substituting this  $\psi$  into equation (3.66) gives us

$$r^2 f''(r) + r f'(r) + ((qr)^2 - n^2) f(r) = 0 \quad (3.70)$$

so that

$$f(r) = A_1 J_n(qr) + B_1 Y_n(qr) \quad (3.71)$$

where  $J_n$ ,  $Y_n$  are Bessel functions and  $A_1$ ,  $B_1$  are arbitrary constants. We shall assume similarly that

$$\phi_j(r, \theta) = g_j(r) e^{in\theta} \quad , \quad (3.72)$$

and find that

$$g_1(r) = A_2 J_n(l_1 r) + B_2 Y_n(l_1 r) \quad (3.73)$$

$$g_2(r) = A_3 J_n(l_2 r) + B_3 Y_n(l_2 r) \quad . \quad (3.74)$$

Now we substitute the expressions

$$\phi(r, \theta) = (g_1(r) + g_2(r)) e^{in\theta} \quad (3.75)$$

$$\psi(r, \theta) = f(r) e^{in\theta} \quad (3.76)$$

into equations (3.49)–(3.51) to get the expressions

$$u_r = \left( g_1'(r) + g_2'(r) + \frac{in}{r} f(r) \right) e^{in\theta + i\gamma z - i\omega t} \quad (3.77)$$

$$u_\theta = \left( \frac{in}{r} (g_1(r) + g_2(r)) - f'(r) \right) e^{in\theta + i\gamma z - i\omega t} \quad (3.78)$$

$$u_z = i(m_1 g_1(r) + m_2 g_2(r)) e^{in\theta + i\gamma z - i\omega t} \quad (3.79)$$

$$= i \left( \gamma g_1(r) - \frac{l_2^2}{\gamma} g_2(r) \right) e^{in\theta + i\gamma z - i\omega t} \quad . \quad (3.80)$$

Here, if we consider only the terms involving  $f$  or  $g_2$ , we find that the displacements have zero divergence, or  $\nabla \cdot (u_r, u_\theta, u_z) = 0$ . This tells us that these terms represent two types of shear wave. On the other hand, if only  $g_1$  terms are considered, we find that  $\nabla \wedge (u_r, u_\theta, u_z) = 0$ , which tells us that these terms represent compressible waves in the solid.

The displacements are now substituted into equations (3.46)–(3.48) to get

$$\begin{aligned} \sigma_{rr} = & \left[ 2in\mu \left( \frac{f'(r)}{r} - \frac{f(r)}{r^2} \right) - \frac{2\mu}{r} (g_1'(r) + g_2'(r)) + \frac{2n^2\mu}{r^2} (g_1(r) + g_2(r)) \right. \\ & \left. + ( - (\lambda + 2\mu)l_1^2 - \lambda\gamma^2 ) g_1(r) + ( - (\lambda + 2\mu)l_2^2 + \lambda l_2^2 ) g_2(r) \right] e^{in\theta + i\gamma z - i\omega t} \quad (3.81) \end{aligned}$$

$$\begin{aligned} \sigma_{r\theta} = \mu & \left[ \frac{2f'(r)}{r} - \frac{2n^2}{r^2} f(r) + q^2 f(r) \right. \\ & \left. + \frac{2in}{r} (g_1'(r) + g_2'(r)) - \frac{2in}{r^2} (g_1(r) + g_2(r)) \right] e^{in\theta + i\gamma z - i\omega t} \end{aligned} \quad (3.82)$$

$$\sigma_{rz} = \mu \left[ 2i\gamma g_1'(r) + i \left( \gamma - \frac{l_2^2}{\gamma} \right) g_2'(r) - \frac{n\gamma}{r} f(r) \right] e^{in\theta + i\gamma z - i\omega t} . \quad (3.83)$$

Now, consider the cylinder depicted in Figure 3.3. For free vibrations of this cylinder,  $\sigma_{rr}$ ,  $\sigma_{r\theta}$  and  $\sigma_{rz}$  must all be zero at  $r = r_1$  and  $r = r_2$ , where  $r_1 = R - h/2$  and  $r_2 = R + h/2$ . This leads to a matrix equation

$$\mathbf{A}\mathbf{c} = 0 \quad (3.84)$$

where  $\mathbf{c} = (A_1, B_1, A_2, B_2, A_3, B_3)^T$ . The characteristic equation, which describes the free motion

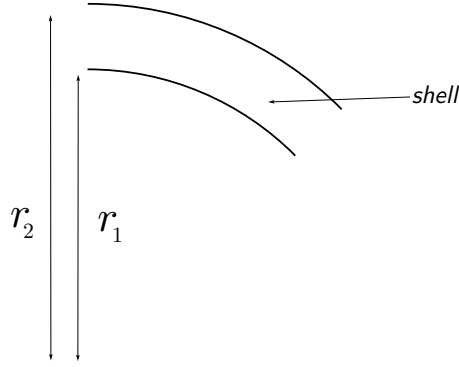


Figure 3.3: Diagram of the thick cylindrical tube

of the cylinder, is given by

$$\det \mathbf{A} = 0 \quad (3.85)$$

Extensive calculation shows that

$$a_{11} = \frac{2in\mu}{r_2^2} (qr_2 J_{n-1}(qr_2) - (n+1)J_n(qr_2)) \quad (3.86)$$

$$a_{13} = \left( \frac{2n(n+1)\mu}{r_2^2} - (\lambda + 2\mu)l_1^2 - \lambda\gamma^2 \right) J_n(l_1 r_2) - \frac{2l_1\mu}{r_2} J_{n-1}(l_1 r_2) \quad (3.87)$$

$$a_{15} = \left( \frac{2n(n+1)\mu}{r_2^2} - 2\mu l_2^2 \right) J_n(l_2 r_2) - \frac{2l_2\mu}{r_2} J_{n-1}(l_2 r_2) \quad (3.88)$$

$$a_{21} = \frac{2\mu q}{r_2} J_{n-1}(qr_2) + \left( q^2\mu - \frac{2n(n+1)\mu}{r_2^2} \right) J_n(qr_2) \quad (3.89)$$

$$a_{23} = \frac{2i\mu n l_1}{r_2} J_{n-1}(l_1 r_2) - \frac{2\mu i n (n+1)}{r_2^2} J_n(l_1 r_2) \quad (3.90)$$

$$a_{25} = \frac{2i\mu n l_2}{r_2} J_{n-1}(l_2 r_2) - \frac{2\mu i n (n+1)}{r_2^2} J_n(l_2 r_2) \quad (3.91)$$

$$a_{31} = -\frac{n\mu\gamma}{r_2} J_n(qr_2) \quad (3.92)$$

$$a_{33} = 2i\mu l_1 \gamma J_{n-1}(l_1 r_2) - \frac{2in\mu\gamma}{r_2} J_n(l_1 r_2) \quad (3.93)$$

$$a_{35} = i\mu l_2 \left( \gamma - \frac{l_2^2}{\gamma} \right) J_{n-1}(l_2 r_2) - \frac{in\mu(\gamma^2 - l_2^2)}{\gamma r_2} J_n(l_2 r_2) \quad (3.94)$$

In addition,  $a_{12}$  is the same as  $a_{11}$  but using Bessel functions of the second kind ( $Y_n$ ) rather than the first kind ( $J_n$ ), similarly for  $a_{14}$  compared with  $a_{13}$  and so on. For the final three rows of the matrix, we use the same entries as for the first three rows, but now  $r_2$  is replaced by  $r_1$ .

### 3.2.1.1 Motion independent of $z$

For  $z$ -independent motion, we assume that the axial wavelength tends to infinity, or, equivalently, that  $\gamma \rightarrow 0$ . We find that  $q \rightarrow k_s^2$ ,  $l_1^2 \rightarrow k_c^2$  and  $l_2^2 \rightarrow k_s^2$ . Because the Bessel functions only take positive argument, we must have

$$q = k_s, \quad l_1 = k_c, \quad \text{and} \quad l_2 = k_s \quad (3.95)$$

when  $\gamma = 0$ .

As an aside, if we multiply the third and sixth rows of equation (3.84) by  $\gamma/(\gamma^2 - l_2^2)$  and let  $\gamma \rightarrow 0$ , we find that the entries  $a_{31}$ ,  $a_{32}$ ,  $a_{33}$ ,  $a_{34}$ ,  $a_{61}$ ,  $a_{62}$ ,  $a_{63}$  and  $a_{64}$  all become zero. This means that the characteristic equation (3.85) decomposes into

$$\det \mathbf{A}_1 \det \mathbf{A}_2 = 0 \quad (3.96)$$

The equation  $\det \mathbf{A}_1 = 0$  corresponds to plane-strain vibrations of the cylinder, and  $\det \mathbf{A}_2 = 0$  to longitudinal vibrations involving only  $u_z$ . When the motion is independent of  $z$ , equation (3.96) tells us that the two types of motion have become uncoupled.

With these alterations, the entries of the matrix  $\mathbf{A}$  are now given by

$$a_{11} = \frac{2in\mu}{r_2^2} (k_s r_2 J_{n-1}(k_s r_2) - (n+1) J_n(k_s r_2)) \quad (3.97)$$

$$a_{13} = \left( \frac{2n(n+1)\mu}{r_2^2} - (\lambda + 2\mu)k_c^2 \right) J_n(k_c r_2) - \frac{2k_c\mu}{r_2} J_{n-1}(k_c r_2) \quad (3.98)$$

$$a_{15} = \left( \frac{2n(n+1)\mu}{r_2^2} - 2\mu k_s^2 \right) J_n(k_s r_2) - \frac{2k_s\mu}{r_2} J_{n-1}(k_s r_2) \quad (3.99)$$

$$a_{21} = \frac{2\mu k_s}{r_2} J_{n-1}(k_s r_2) + \left( k_s^2 \mu - \frac{2n(n+1)\mu}{r_2^2} \right) J_n(k_s r_2) \quad (3.100)$$

$$a_{23} = \frac{2i\mu n k_c}{r_2} J_{n-1}(k_c r_2) - \frac{2\mu in(n+1)}{r_2^2} J_n(k_c r_2) \quad (3.101)$$

$$a_{25} = \frac{2i\mu n k_s}{r_2} J_{n-1}(k_s r_2) - \frac{2\mu in(n+1)}{r_2^2} J_n(k_s r_2) \quad (3.102)$$

$$a_{31} = a_{33} = 0 \quad (3.103)$$

$$a_{35} = i\mu k_s J_{n-1}(k_s r_2) - \frac{in\mu}{r_2} J_n(k_s r_2) \quad (3.104)$$

using the same pattern for the other entries, as outlined in the previous part.

### 3.2.2 Water-filled Hollow Cylinder

Now we shall assume that the space in  $0 < r < r_1$  is filled with water, and a pressure  $P e^{iks - i\omega t}$  applied to the exterior,  $r = r_2$ . As for the thin shell theory, we note that  $s = r_2\theta$ , and that  $kr_2$  needs to be an integer. For the remainder of this section we shall write  $n$  for  $kr_2$ .

We have already found that the pressure in the water will be given by equation (3.35), or

$$p = (\tilde{A}J_n(k_0r) + \tilde{B}Y_n(k_0r))e^{in\theta - i\omega t} \quad (3.105)$$

where  $\tilde{A}$ ,  $\tilde{B}$  are constants. However, the pressure must be finite at  $r = 0$ , so  $\tilde{B} = 0$ . We also let the pressure at  $r = r_1$  be  $p_l e^{in\theta - i\omega t}$ , so that

$$p = p_l \frac{J_n(k_0r)}{J_n(k_0r_1)} e^{in\theta - i\omega t} \quad (3.106)$$

Now we use Euler's equation (3.29) at  $r = r_1$ , to obtain, finally,

$$p_l = X \mathbf{b} \cdot \begin{pmatrix} A_1 \\ B_1 \\ A_2 \\ B_2 \\ A_3 \\ B_3 \end{pmatrix} \quad (3.107)$$

where

$$X = \frac{J_n(k_0r_1)}{k_0 J'_n(k_0r_1)} \quad (3.108)$$

and

$$\mathbf{b} = \begin{pmatrix} \frac{\rho_0 \omega^2 i n}{r_1} J_n(k_s r_1) \\ \frac{\rho_0 \omega^2 i n}{r_1} Y_n(k_s r_1) \\ \rho_0 \omega^2 k_c J'_n(k_c r_1) \\ \rho_0 \omega^2 k_c Y'_n(k_c r_1) \\ \rho_0 \omega^2 k_s J'_n(k_s r_1) \\ \rho_0 \omega^2 k_s Y'_n(k_s r_1) \end{pmatrix} \quad (3.109)$$

In this situation, equation (3.84) is replaced by

$$\mathbf{A} \begin{pmatrix} A_1 \\ B_1 \\ A_2 \\ B_2 \\ A_3 \\ B_3 \end{pmatrix} = \begin{pmatrix} -P \\ 0 \\ 0 \\ -p_l \\ 0 \\ 0 \end{pmatrix} \quad (3.110)$$

But from the expression for  $p_l$  in equation (3.107) above, we can form a matrix  $\mathbf{B}$  whose entries are the same as those of  $\mathbf{A}$ , except in the fourth row where they equal  $a_{ij} + X b_j$ , where  $b_j$  are the

entries of the vector  $\mathbf{b}$ . This then allows us to form the linear system

$$\mathbf{B} \begin{pmatrix} A_1 \\ B_1 \\ A_2 \\ B_2 \\ A_3 \\ B_3 \end{pmatrix} = \begin{pmatrix} -P \\ 0 \\ 0 \\ 0 \\ 0 \\ 0 \end{pmatrix} . \quad (3.111)$$

This is solved numerically, then  $p_l$  is found from equation (3.107). The pressure in the fluid is then given by equation (3.106).

### 3.2.3 Inclusion of a Rigid Cylinder

In the same way as for the thin cylindrical shell, we will now include a rigid cylinder in the interior of the thick cylindrical tube, as shown in Figure 3.4, where  $r_0 = R - h/2 - h_0$ . The exterior,  $r = r_2$ , is still given an applied pressure  $P e^{in\theta - i\omega t}$ .

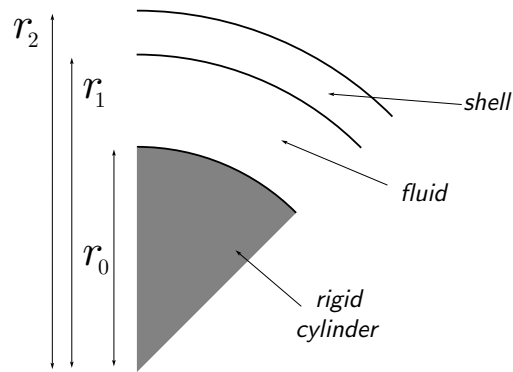


Figure 3.4: Diagram of the thick cylindrical tube with a rigid cylinder

Returning to equation (3.105), we demand that

$$\left. \frac{\partial p}{\partial r} \right|_{r=r_0} = 0 \quad (3.112)$$

and

$$p|_{r=r_1} = p_l . \quad (3.113)$$

This tells us that

$$p = p_l \frac{J_n(k_0 r) + X_1 Y_n(k_0 r)}{J_n(k_0 r_1) + X_1 Y_n(k_0 r_1)} \quad (3.114)$$

where

$$X_1 = -\frac{k_0 J'_n(k_0 r_0)}{k_0 Y'_n(k_0 r_0)} . \quad (3.115)$$

From here on, the analysis follows the pattern of the previous section. The equation of motion of the thick shell is given by equation (3.110), but  $p_l$  is given by equation (3.107), where in this case

$$X = \frac{J_n(k_0 r_1) + X_1 Y_n(k_0 r_1)}{k_0 J'_n(k_0 r_1) + k_0 X_1 Y'_n(k_0 r_1)} . \quad (3.116)$$

We therefore transform the system to equation (3.111) in the same way as before (with the new value of  $X$ ) and we solve it numerically. Then  $p_l$  is found from equation (3.107), and the pressure in the water is finally given by equation (3.114).

### 3.3 Results and Discussion

We will consider first the results from the thin shell theory. The pressure on the inner surface of the shell without the rigid cylinder — as a function of  $k$  — is seen in Figure A.5, with  $R = 5$  m as in Table 1.2. We clearly see a peak at the bending wavenumber of the shell,  $k = 29.3 \text{ m}^{-1}$ , together with an irregular pattern when the excitation wavenumber is supersonic. When a rigid cylinder is included, (Figure A.6), the graph becomes much clearer (not only because we have increased the resolution here: although the excitation wavenumbers must be of the form  $n/r_2$  for integer  $n$ , we can interpolate these points by considering the wavenumbers in between). The most striking feature of this graph is its similarity to the graph in Figure A.3. They are virtually identical except for a slender peak near the longitudinal wavenumber of the shell. This must therefore be a manifestation of the coupling of modes by the shell's curvature. We thus have peaks due to both the bending and longitudinal modes of the shell, and two peaks due to resonance effects in the fluid.

As the offset  $h_0$  is increased, the number of resonant peaks increases, which is true for the infinite flat plate as well as the cylindrical shell. Therefore, as the rigid cylinder becomes smaller, the peaks become closer together, until we obtain an irregular pattern of peaks, as in the case with no rigid cylinder. We deduce, therefore, that the irregular pattern seen in the no-rigid-cylinder case is due to resonances in the interior of the cylindrical shell, and there is a large number of these since  $k_0 R$  is large: around 100 for our choice of constants.

The graph on the inner surface of the thick shell without a rigid cylinder, shown in Figure A.7 is very similar to that of the thin shell, displaying the irregular region caused by resonance effects. When the rigid cylinder is included (Figure A.8), the graph shares some characteristics with that of the thin shell theory. We still have a peak at the bending wavenumber, and two peaks due to resonant effects. The peak due to the longitudinal motion is more pronounced in the thick shell graph than in that of the thin shell, and occurs at a lower wavenumber (as indeed, does the peak due to the bending mode). The origin of the two peaks of lowest wavenumber are uncertain.

All four graphs are calculated at an offset  $h_0$  from the cylindrical shell.

## Chapter 4

# Effects of a Finite Plate

In addition to curvature, effects due to the vibration of plate edges have been suggested as an explanation for the increased noise levels at certain bearings. We will investigate this effect in this chapter, using numerical methods to solve the equations.

### 4.1 Analysis of a Finite Plate

#### 4.1.1 Problem Formulation

The configuration of the problem is depicted in Figure 4.1. We assume that a thin plate of length  $2l$  in the  $x$ -direction is attached to two semi-infinite rigid plates at  $x = \pm l$ . As in previous chapters, we will apply a sinusoidally varying pressure  $Pe^{ikx-i\omega t}$  to the upper edge, and measure the pressure at a distance  $h_0$  from the plate in water on the other side of the plate. We assume that the plate is infinite in the  $y$ -direction.

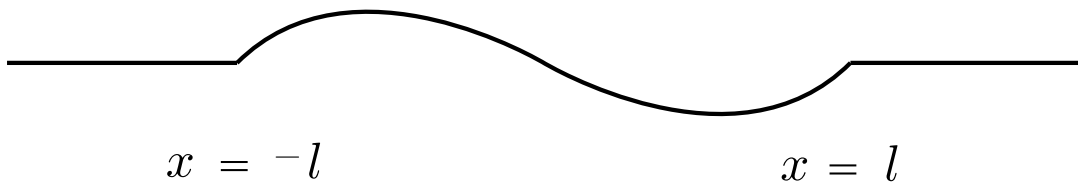


Figure 4.1: A finite plate

Recalling the mechanism by which the sonar dome is attached to the free-flooding structure, in Figure 1.4, we deduce that an appropriate approximation to the boundary condition for the plate edges is a *hinged* condition, that is, where we prescribe zero displacement and zero moment at the edges. The simplest alternative would be a clamped condition, where zero gradient is prescribed together with zero displacement.

The equations to be solved are

$$\nabla^2 p + k_0^2 p = 0 \quad (4.1)$$

in  $z < 0$  and for  $-\infty < x < \infty$ , with

$$\left. \frac{\partial p}{\partial z} \right|_{z=0} = \begin{cases} \rho_0 \omega^2 w(x) & x \in [-l, l] \\ 0 & \text{otherwise} \end{cases} \quad (4.2)$$

where  $w(x)$  satisfies

$$\frac{Eh}{12(1-\nu^2)} \frac{d^4 w}{dx^4} - \rho_p h \omega^2 w(x) = -P e^{ikx} + p(x, 0) \quad (4.3)$$

with

$$w(-l) = w''(-l) = w(l) = w''(l) = 0 \quad (4.4)$$

Note that we have assumed that both the pressure in the water, and the displacement of the plate have a harmonic time dependence  $e^{-i\omega t}$ , and have already eliminated this factor.

Attempts to solve this problem in a similar way to previous chapters are doomed to failure, so we must try a different approach. One solution technique is suggested by Tayler [19]. Firstly, we find a solution of equation (4.1) which corresponds to a line source at  $(x, z) = (s, 0)$ . This is given by the equation

$$\frac{\partial^2 p}{\partial r^2} + \frac{1}{r} \frac{\partial p}{\partial r} + k_0^2 p = \delta(\mathbf{r}) \quad (4.5)$$

where  $\mathbf{r} = (x, z) - (s, 0)$ ,  $r = |\mathbf{r}|$  and  $\delta(\mathbf{r})$  is the Dirac delta function. The solution to this equation is given by

$$p(r) = AJ_0(k_0 r) + BY_0(k_0 r) \quad (4.6)$$

where  $A, B$  are constants and  $J_0, Y_0$  are the Bessel functions. An alternative solution is found if we define the Hankel functions by

$$H_0^{(1)}(x) = J_0(x) + iY_0(x) \quad (4.7)$$

$$H_0^{(2)}(x) = J_0(x) - iY_0(x) \quad (4.8)$$

(see Abramowitz and Stegun, [1]) and thus

$$p(r) = \tilde{A}H_0^{(1)}(k_0 r) + \tilde{B}H_0^{(2)}(k_0 r) \quad (4.9)$$

for constants  $\tilde{A}, \tilde{B}$ .

We need to ensure that as  $r \rightarrow \infty$ , we have outgoing waves — that is,  $p \sim g(r)e^{ik_0 r - i\omega t}$  for some  $g(r)$ . Abramowitz and Stegun [1] tell us that in this limit,

$$H_0^{(1)}(k_0 r) \sim \sqrt{\frac{2}{\pi k_0 r}} e^{i(k_0 r - \pi/4)} \quad (4.10)$$

$$H_0^{(2)}(k_0 r) \sim \sqrt{\frac{2}{\pi k_0 r}} e^{-i(k_0 r - \pi/4)} \quad (4.11)$$

so that of these, only  $H_0^{(1)}(k_0 r)$  can satisfy this radiation condition. Hence

$$p(r) = \tilde{A} H_0^{(1)}(k_0 r) \quad . \quad (4.12)$$

Now, any distribution of line sources along  $z = 0$ , with some density  $f(x)$ , will also be a solution of equation (4.1). We can therefore write

$$p(x, z) = \tilde{A} \int_{-\infty}^{\infty} f(s) H_0^{(1)}\left(k_0 \sqrt{(x-s)^2 + z^2}\right) ds \quad . \quad (4.13)$$

We choose  $\tilde{A}f(x)$  so that the pressure satisfies equation (4.2). In this case  $\tilde{A}f(x) = \frac{1}{2}i\rho_0\omega^2 w(x)$ , and hence

$$p(x, z) = \frac{i}{2}\rho_0\omega^2 \int_{-l}^l w(s) H_0^{(1)}\left(k_0 \sqrt{(x-s)^2 + z^2}\right) ds \quad . \quad (4.14)$$

Taylor, in his explanation, had chosen a time factor of  $e^{i\omega t}$  so was mistaken in his choice of  $H_0^{(1)}(\cdot)$  as the outgoing wave solution. The result given here is correct for a time dependence of  $e^{-i\omega t}$ .

This means that the equation for  $w(x)$  then becomes

$$\frac{d^4 w}{dx^4} = a_1 w(x) - a_2 e^{ikx} + a_3 \int_{-l}^l w(s) H_0^{(1)}(k_0 |x-s|) ds \quad (4.15)$$

with boundary conditions (4.4), and where

$$a_1 = \frac{12\rho_p(1-\nu^2)\omega^2}{Eh^2} \quad (4.16)$$

$$a_2 = \frac{12(1-\nu^2)P}{Eh^3} \quad (4.17)$$

$$a_3 = \frac{6i\rho_0\omega^2(1-\nu^2)}{Eh^3} \quad . \quad (4.18)$$

We now need to solve this equation for  $w(x)$  and substitute the solution into equation (4.14) at  $z = -h_0$ . Unfortunately there is no obvious way to do this analytically, so we must approach the problem with a numerical method.

#### 4.1.2 The Finite Difference Method

Firstly, we create a mesh by dividing the domain  $[-l, l]$  into  $m$  sections. Then the gridpoints will be given by

$$x_j = \left(\frac{2j}{m} - 1\right) l \quad (4.19)$$

for  $j = 0, \dots, m$ . Then let  $w_j$  be the numerical approximation to  $w(x_j)$ . The step size is given by  $\Delta x = 2l/m$ .

Now, it seems reasonable to approximate the integral in equation (4.15) using the trapezium rule, on the grid defined above. However, we note that the Hankel functions  $H_0^{(i)}(\xi)$  have a logarithmic singularity at  $\xi = 0$ , and if we used the same gridpoints for the integral and the differential equation, our numerical method would undoubtedly fail. Instead, we use the end gridpoints  $x_0$  and  $x_m$  together

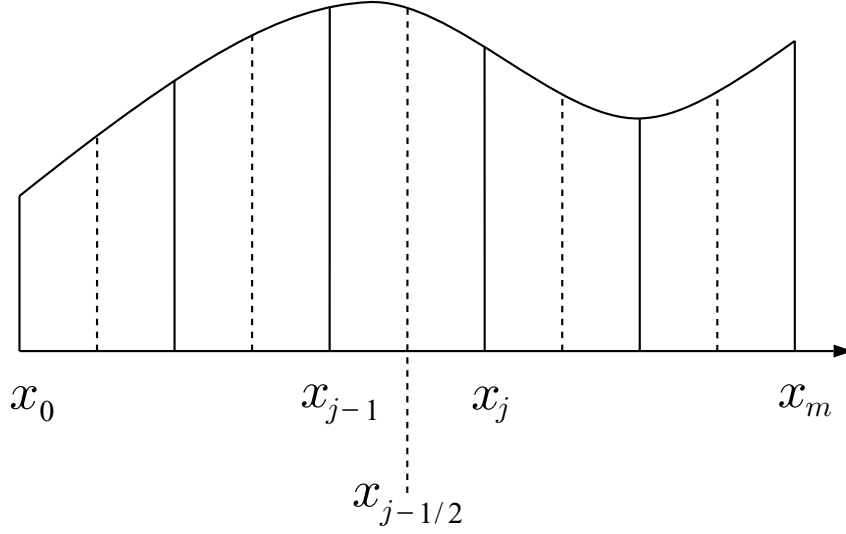


Figure 4.2: Grid for the numerical scheme

with  $x_{j-1/2}$  for  $j = 1, \dots, m$ ; the dotted lines in Figure 4.2. There is no problem with singularities at the end gridpoints because  $w_0$  and  $w_m$  are set to zero by equation (4.4).

The trapezium rule approximation on this grid is given by

$$\int_{-l}^l w(s)H_0^{(1)}(k_0|x-s|) ds \approx \frac{3\Delta x}{4} \left[ w(x_{1/2})H_0^{(1)}(k_0|x-x_{1/2}|) + w(x_{m-1/2})H_0^{(1)}(k_0|x-x_{m-1/2}|) \right] + \Delta x \sum_{j=1}^{m-2} w(x_{j+1/2})H_0^{(1)}(k_0|x-x_{j+1/2}|) \quad (4.20)$$

We then approximate

$$w(x_{j+1/2}) \approx \frac{w_j + w_{j+1}}{2} \quad (4.21)$$

which means that the integral in equation (4.20) is approximated by

$$\mathbf{h}(x) \cdot \begin{pmatrix} w_1 \\ \vdots \\ w_{m-1} \end{pmatrix} = \left[ \frac{3\Delta x}{8}H_0^{(1)}(k_0|x-x_{1/2}|) + \frac{\Delta x}{2}H_0^{(1)}(k_0|x-x_{1+1/2}|) \right] w_1 + \sum_{j=2}^{m-2} \left[ \frac{\Delta x}{2}H_0^{(1)}(k_0|x-x_{j-1/2}|) + \frac{\Delta x}{2}H_0^{(1)}(k_0|x-x_{j+1/2}|) \right] w_j + \left[ \frac{\Delta x}{2}H_0^{(1)}(k_0|x-x_{m-3/2}|) + \frac{3\Delta x}{8}H_0^{(1)}(k_0|x-x_{m-1/2}|) \right] w_{m-1} \quad (4.22)$$

Now we discretise equation (4.15). Firstly, we set  $v(x) = w''(x)$ , thus obtaining a system

$$w''(x) = v(x) \quad (4.23)$$

$$v''(x) = a_1 w(x) - a_2 e^{ikx} + a_3 \int_{-l}^l w(s)H_0^{(1)}(k_0|x-s|) ds \quad (4.24)$$

The second derivatives are then approximated by finite differences, and the integral by the modified trapezium method above, to give a recursion relation

$$\frac{w_{j-1} - 2w_j + w_{j+1}}{\Delta x^2} = v_j \quad (4.25)$$

$$\frac{v_{j-1} - 2v_j + v_{j+1}}{\Delta x^2} = a_1 w_j - a_2 e^{ikx_j} + a_3 \mathbf{h}(x_j) \cdot \begin{pmatrix} w_1 \\ \vdots \\ w_{m-1} \end{pmatrix} \quad (4.26)$$

for  $j = 1, \dots, m-1$ , and with  $w_0 = w_m = v_0 = v_m = 0$ .

We eventually obtain a matrix equation,

$$\mathbf{M} \begin{pmatrix} w_1 \\ \vdots \\ w_{m-1} \end{pmatrix} = -a_2 \begin{pmatrix} e^{ikx_1} \\ \vdots \\ e^{ikx_{m-1}} \end{pmatrix} \quad (4.27)$$

where  $\mathbf{M} = \mathbf{A}^2 - \mathbf{B}$ , for

$$\mathbf{A} = \frac{1}{\Delta x^2} \begin{pmatrix} -2 & 1 & & & 0 \\ 1 & -2 & \ddots & & \\ 0 & 1 & \ddots & 1 & 0 \\ & & \ddots & -2 & 1 \\ 0 & & & 1 & -2 \end{pmatrix} \quad (4.28)$$

and

$$\mathbf{B} = a_1 \mathbf{I} + a_3 \begin{pmatrix} \mathbf{h}(x_1)^T \\ \vdots \\ \mathbf{h}(x_{m-1})^T \end{pmatrix} \cdot \quad (4.29)$$

Here,  $\mathbf{I}$  denotes the unit matrix.

The matrix equation is solved, and substituted into the trapezium rule approximation of equation (4.14) at  $z = -h_0$ , with no danger from singularities in this case. The pressure then becomes

$$p(x, -h_0) \approx i\rho_0 \omega^2 \Delta x \sum_{j=1}^{m-1} w_j H_0^{(1)} \left( k_0 \sqrt{(x-x_j)^2 + h_0^2} \right) \quad (4.30)$$

### 4.1.3 Inclusion of a Rigid Boundary

Now we consider the same problem as before, but with a rigid boundary at  $z = -h_0$ . Without this boundary, we found that the pressure due to a line source at  $(x, z) = (s, 0)$  was

$$p(x, z) = \tilde{A} H_0^{(1)} \left( k_0 \sqrt{(x-s)^2 + z^2} \right) \quad (4.31)$$

To take account of the rigid boundary, however, we make use of the method of images. This method tells us that if we require

$$\left. \frac{\partial p}{\partial z} \right|_{z=-h_0} = 0 \quad (4.32)$$

then we must have a source of equal strength placed at  $(x, z) = (s, -2h_0)$ . Thus the resultant pressure field is given by

$$p(x, z) = \tilde{A} \left[ H_0^{(1)} \left( k_0 \sqrt{(x-s)^2 + z^2} \right) + H_0^{(1)} \left( k_0 \sqrt{(x-s)^2 + (z+2h_0)^2} \right) \right] . \quad (4.33)$$

As before, we now consider a distribution of sources, and scale appropriately to give

$$p(x, z) = \frac{i}{2} \rho_0 \omega^2 \int_{-l}^l w(s) \left[ H_0^{(1)} \left( k_0 \sqrt{(x-s)^2 + z^2} \right) + H_0^{(1)} \left( k_0 \sqrt{(x-s)^2 + (z+2h_0)^2} \right) \right] ds \quad (4.34)$$

The numerical scheme for the solution of this problem, with the altered equation for  $w(x)$ , is now of exactly the same form as before.

## 4.2 An Alternative Method

The method used in the previous section, although giving satisfactory results, was slow to converge, possibly due to the fact that we were trying to integrate singular functions numerically. It was also a slow method because we had to solve equations with full matrices. An alternative approach is to turn the system in equations (4.23) and (4.24) into a system of integral equations, which should be ‘better behaved’ due to the absence of discontinuities.

Equation (4.23) with boundary conditions  $w(-l) = w(l) = 0$  has solution

$$w(x) = \int_{-l}^l G(x, \xi) v(\xi) d\xi \quad (4.35)$$

where the Green’s function  $G(x, \xi)$  satisfies

$$\frac{d^2 G}{dx^2} = \delta(\xi - x) \quad (4.36)$$

$$G(-l, \xi) = G(l, \xi) = 0 \quad (4.37)$$

where  $\delta(x)$  is the Dirac delta function. The solution is given by

$$G(x, \xi) = \begin{cases} \frac{(\xi + l)(x - l)}{2l} & \text{if } \xi \leq x \\ \frac{(\xi - l)(x + l)}{2l} & \text{if } x < \xi \end{cases} \quad (4.38)$$

for  $x, \xi \in [-l, l]$ .

In a similar way, equation (4.24) has solution

$$v(x) = \int_{-l}^l G(x, \xi) \left[ a_1 w(\xi) + a_3 \int_{-l}^l w(s) H_0^{(1)}(k_0 |\xi - s|) ds - a_2 e^{ik\xi} \right] d\xi \quad (4.39)$$

for the same Green’s function  $G(x, \xi)$ . We can interchange the variables of integration in the double integral, to get

$$v(x) = \int_{-l}^l \left[ (a_1 G(x, \xi) + a_3 K(x, \xi)) w(\xi) - a_2 G(x, \xi) e^{ik\xi} \right] d\xi \quad (4.40)$$

where

$$K(x, \xi) = \int_{-l}^l G(x, s) H_0^{(1)}(k_0 |\xi - s|) ds \quad . \quad (4.41)$$

This kernel  $K(x, \xi)$  should be continuous, because we are integrating a logarithmic singularity multiplied with a linear function. In fact,

$$\begin{aligned} \int_0^z (a + bt) H_0^{(1)}(k_0 t) dt &= a \left[ z H_0^{(1)}(k_0 z) - \frac{z\pi}{2} \left( H_0^{(1)}(k_0 z) \mathbf{H}_1(k_0 z) - H_1^{(1)}(k_0 z) \mathbf{H}_0(k_0 z) \right) \right] \\ &\quad + \frac{bz}{k_0} H_1^{(1)}(k_0 z) \end{aligned} \quad (4.42)$$

where  $\mathbf{H}_\nu(z)$  is a *Struve function*. This integral can be verified by using the identities (see, for example, Abramowitz and Stegun, [1])

$$\frac{d}{dz} H_0^{(1)}(z) = -H_1^{(1)}(z) \quad (4.43)$$

$$\frac{d}{dz} H_1^{(1)}(z) = H_0^{(1)}(z) - \frac{1}{z} H_1^{(1)}(z) \quad (4.44)$$

$$\frac{d}{dz} \mathbf{H}_0(z) = \frac{2}{\pi} - \mathbf{H}_1(z) \quad (4.45)$$

$$\frac{d}{dz} \mathbf{H}_1(z) = \mathbf{H}_0(z) - \frac{1}{z} \mathbf{H}_1(z) \quad . \quad (4.46)$$

Therefore,  $K(x, \xi)$  can be found in terms of Hankel and Struve functions.

Numerical procedures for the computation of the Struve functions were obtained from the website [http://ceta.mit.edu/comp\\_spec\\_func/](http://ceta.mit.edu/comp_spec_func/). The files used were `mstvh0.m` and `mstvh1.m`, both of which are Matlab implementations of algorithms contained in the book by Zhang and Jin [20] and thus are copyrighted.

For the numerical scheme, we write equations (4.35) and (4.40) as matrix equations, using the trapezium rule to discretise the integrals (having negated the problem of singularities). In other words,

$$\begin{pmatrix} w_1 \\ \vdots \\ w_{m-1} \end{pmatrix} = \mathbf{A} \begin{pmatrix} v_1 \\ \vdots \\ v_{m-1} \end{pmatrix} \quad (4.47)$$

$$\begin{pmatrix} v_1 \\ \vdots \\ v_{m-1} \end{pmatrix} = \mathbf{B} \begin{pmatrix} w_1 \\ \vdots \\ w_{m-1} \end{pmatrix} + \begin{pmatrix} f_1 \\ \vdots \\ f_{m-1} \end{pmatrix} \quad (4.48)$$

for matrices  $\mathbf{A} = (a_{ij})$ ,  $\mathbf{B} = (b_{ij})$  and vector  $(f_1, \dots, f_{m-1})^T$  given by

$$a_{ij} = \Delta x G(x_i, x_j) \quad (4.49)$$

$$b_{ij} = \Delta x (a_1 G(x_i, x_j) + a_3 K(x_i, x_j)) \quad (4.50)$$

$$f_j = -a_2 \Delta x \sum_{p=1}^{m-1} G(x_j, x_p) e^{ikx_p} \quad . \quad (4.51)$$

Solving the integral equations gives us

$$(\mathbf{I} - \mathbf{AB}) \begin{pmatrix} w_1 \\ \vdots \\ w_{m-1} \end{pmatrix} = \mathbf{A} \begin{pmatrix} f_1 \\ \vdots \\ f_{m-1} \end{pmatrix} \quad (4.52)$$

which is solved numerically. Here  $\mathbf{I}$  denotes the unit matrix. The pressure at  $h_0$  from the boundary is then given by equation (4.30).

This routine confirmed the results obtained by the first method. However, the time taken to calculate the Struve functions meant that overall, this integral equation method was considerably slower than the first method.

When a rigid boundary is included behind the finite plate, the system of integral equations (4.35) and (4.40) is exactly the same, except for the fact that the kernel  $K(x, \xi)$  is now given by

$$K(x, \xi) = \int_{-l}^l G(x, s) \left[ H_0^{(1)}(k_0|\xi - s|) + H_0^{(1)}\left(\sqrt{(\xi - s)^2 + 4h_0^2}\right) \right] ds \quad . \quad (4.53)$$

Unfortunately, this can not be easily converted to a closed form expression, as in the case with no rigid boundary. However, the second term in the integral above is not singular, so the kernel could be approximated by a hybrid method — the first integral has already been computed, and the second could be approximated by the trapezium rule.

### 4.3 Results and Discussion

We will first consider the finite plate without a rigid boundary. The length  $l$  was chosen to be 5 m so that the plate was the same size as the edge  $CD$  introduced in section 1.1. The graph of the pressure as a function of the excitation wavenumber, measured at an offset  $h_0$  to the plate, is shown in Figure A.9. The graph shows the average absolute pressure, not measured in decibels as was the case before. We see a peak at the acoustic wavenumber and one at the bending wavenumber, in the same way as infinite thin plate theory has predicted. However, the size of the peak at the bending wavenumber,  $k \approx 34 \text{ m}^{-1}$ , was much higher than anticipated — it was expected to be attenuated, given that  $34 \text{ m}^{-1}$  is a subsonic wavenumber. It was felt that this warranted further exploration, so the profile of the pressure at  $h_0$  from the plate, and the plate displacement itself, were drawn at this wavenumber. The results are shown in Figure A.10 and Figure A.12 respectively.

There are two conclusions to be drawn from these graphs. The first is that the greatest pressure fluctuations are seen near the edges,  $x = \pm 5 \text{ m}$ . This shows us that diffraction from the edges of the plate is having a significant effect on the pressure in the fluid beneath. The reason for this is that the plate displacement  $w(x)$ , from Figure A.12, has a dominant mode proportional to  $\sin kx$ , where  $k \approx 34 \text{ m}^{-1}$ . This means that the integral in equation (4.14) is effectively a Fourier transform of the function  $\phi(s)$  which is zero if  $|s| > l$  and  $H_0^{(1)}\left(\sqrt{(x-s)^2 + z^2}\right)$  if  $|s| < l$ . The integrand has no points of stationary phase since  $k > k_0$ , which implies that the dominant contributions to the

pressure  $p$  come from the points of discontinuity of  $\phi(s)$ , which are at the endpoints  $x = \pm l$  (see Lighthill [11]).

Secondly, and perhaps most interesting, is the difference in wavenumber between the plate displacement and the pressure. The former has a wavenumber consistent with the excitation wavenumber,  $k \approx 34 \text{ m}^{-1}$ , but the latter has a wavenumber of around  $19.5 \text{ m}^{-1}$ . This is because the plate's vibrations are a superposition of vibrations at different wavenumbers. We see that the dominant vibration is that due to the excitation wavenumber. However, this wavenumber is subsonic and so it will attenuate as we move into the fluid. The wavenumber  $19.5 \text{ m}^{-1}$ , however, is supersonic so no attenuation will take place. Therefore, by the time the vibrations reach  $h_0$ , the dominant vibration will be at a supersonic wavenumber, as shown in Figure A.10.

We will now consider the effect of the rigid boundary. The graph of the pressure as a function of the excitation wavenumber is shown in Figure A.13. We see the peak due to the bending motion of the plate at  $k \approx 34 \text{ m}^{-1}$  again, and a peak due to resonance effects at  $k \approx 18 \text{ m}^{-1}$ . The profile of the pressure at  $h_0$  from the plate, and the plate displacement itself are shown in Figure A.14 and Figure A.16 respectively. They show the same characteristics as the equivalent graphs without the rigid boundary — with two exceptions. Firstly, the effect due to the edges of the plate occurs over a wider interval, presumably because of the reflection of the diffracted field by the rigid boundary. Secondly, the apparent wavenumber of the pressure at the bending wavenumber is now approximately  $17.5 \text{ m}^{-1}$ .

## Chapter 5

# Viscoelastic Effects

In general, materials are not perfectly elastic. When such materials are deformed, some of the energy applied is dissipated. This can be explained by the fact that materials can, on long timescales, flow like a viscous fluid. Conversely, on a short timescale, some viscous fluids have elastic properties. This chapter will investigate the effects that arise when this behaviour — viscoelasticity — is taken into account.

### 5.1 The Complex Modulus

We shall consider materials that are not purely elastic, but are still linear. We will let  $e(t)$  be some component of strain, and  $\sigma(t)$  be some component of stress, both of which will vary with time  $t$ . Then, for a linear, time-invariant viscoelastic material, the relation

$$e(t) = \int_0^\infty \gamma(\tau)\sigma(t-\tau) d\tau \quad (5.1)$$

will hold for some function  $\gamma(t)$ . This is to be compared with the equation for a purely elastic material,  $e(t) = G\sigma(t)$  for some constant  $G$ .

Now, we will assume that both the strain and the stress are harmonic in time,

$$\sigma(t) = \Re(\hat{\sigma}e^{-i\omega t}) \quad (5.2)$$

$$e(t) = \Re(\hat{e}e^{-i\omega t}) \quad (5.3)$$

for complex  $\hat{\sigma}$ ,  $\hat{e}$ ; and where  $\Re$  denotes the real part. Substituting these into equation (5.1) leads to

$$\hat{e}e^{-i\omega t} = \hat{\sigma} \int_0^\infty \gamma(\tau)e^{-i\omega(t-\tau)} d\tau \quad (5.4)$$

$$= \hat{\sigma}e^{-i\omega t} \int_0^\infty \gamma(\tau)e^{i\omega\tau} d\tau \quad (5.5)$$

Therefore, if we define

$$\Gamma(\omega) = \int_0^\infty \gamma(\tau)e^{i\omega\tau} d\tau \quad (5.6)$$

to be the *complex compliance* or *dynamic compliance*, then we have a relation between  $\hat{\sigma}$  and  $\hat{\epsilon}$ ,

$$\hat{\epsilon} = \Gamma(\omega)\hat{\sigma} \quad . \quad (5.7)$$

The fact that energy must be dissipated in a complete cycle is equivalent to requiring that  $\Gamma$  has non-negative imaginary part. We can therefore write

$$\Gamma = |\Gamma|e^{i\delta} \quad (5.8)$$

where  $\delta$  is defined to be the loss angle. If equation (5.7) is expressed in terms of a stiffness or modulus  $M$ , so that  $\hat{\sigma} = M\hat{\epsilon}$ , then  $M = 1/\Gamma$  has non-positive imaginary part, leading to  $M = |M|e^{-i\delta}$ . (Some authors consider a harmonic time dependence of  $e^{i\omega t}$ , which leads to  $\delta$  being given by  $M = |M|e^{i\delta}$ .)

For more general stresses and strains, given in tensor form, the equivalent condition on  $\Gamma$ , the compliance matrix, and  $M = \Gamma^{-1}$ , the stiffness matrix, is that the imaginary part of  $\Gamma$  should be positive semidefinite (for  $\omega > 0$ ) and therefore that the imaginary part of  $M$  be negative semidefinite. Here,  $M$  and  $\Gamma$  are both symmetric matrices.

Therefore, if we wish to extend the results obtained in previous chapters to account for viscoelastic effects, we need to replace the Lamé moduli  $\lambda$  and  $\mu$  by the full complex moduli,  $\lambda(1 - i \tan \delta)$  and  $\mu(1 - i \tan \delta)$ .

A full introduction to viscoelasticity theory can be found in Pipkin [14].

## 5.2 Results and Discussion

We shall consider first the effect that the consideration of viscoelastic effects has on the vibration of the infinite thick flat plate. Figure A.17 shows that the peak due to bending plate modes is decreased, but that the peak due to the longitudinal motion has been increased greatly. Thus viscoelastic effects may deliver the higher peak needed at the longitudinal wavenumber. However, this seems unlikely, because when a rigid boundary is included, the graph in Figure A.18 shows that the peak due to longitudinal effects has been greatly decreased, so that in fact there is no longer any peak here. The reason for the increase of the peak without a rigid boundary, compared to the decrease without it, is a matter which needs investigating. The peaks due to resonant effects have been decreased slightly, but not nearly as much as the longitudinal and bending peaks.

Similar results are seen for the graphs of the thin shell (Figure A.19) and thick shell (Figure A.20) with rigid cylinders. In the first case, the peak due to the bending motion has been significantly decreased, and the peak due to longitudinal motion has been completely dissipated, following the pattern of the thick plate with a rigid boundary. Similarly, the graph of the thick shell in this case shows significantly decreased longitudinal and bending peaks, although here we can still see an effect due to longitudinal motion. The resonant peaks in both cases are slightly decreased.

A similar result can be seen in the graphs of the pressure behind a finite plate with and without a rigid boundary, Figures A.21 and A.22 respectively. In the former, the peak at the longitudinal wavenumber is reduced while the acoustic peak has not been reduced at all. In the latter case, the resonant peak is unchanged while the peak at the bending wavenumber has again been reduced.

# Chapter 6

## Conclusions

We will now attempt to ascertain what we have learnt from the previous chapters, and to see how we can apply the results obtained to the problem outlined in the introduction. Following on from this, we will suggest some avenues for further research into the problem.

### 6.1 Interpretation of the Results

It was originally thought that longitudinal effects would be the primary cause behind the elevated noise levels, because of the appearance of signals at bearings which were consistent with the longitudinal number of the sonar dome. Thick plate theory failed to confirm this conjecture, until a rigid boundary at a distance  $h_0$  from the plate was considered. In this situation, the peak due to longitudinal vibrations in the plate was amplified. A second area studied is curvature, and since this couples bending and longitudinal modes of motion, both thin and thick shell theory were expected to show peaks due to longitudinal motion. Indeed, this was recorded, when a rigid cylinder was included inside the shell. (Without this no such pattern can be discerned due to resonance effects in the fluid.) However, when viscoelastic effects in the material are taken into account, the peak due to longitudinal motion disappears in all cases (except for the anomaly in the case of the infinite thick plate). This suggests that longitudinal effects may not be the cause of the rogue signals detected by the hydrophones.

We must therefore consider other candidates to explain the signals. One such candidate is the effect of resonance between the sonar dome and the rigid boundary on which the hydrophones are mounted. This phenomenon appears in all cases considered — the thin and thick infinite plates, the thin and thick cylindrical shells, and also the finite plate. This fact suggests strongly that resonance is the cause of the signals detected by the array, especially as these peaks remain (although slightly diminished) when viscoelastic effects are considered. While the peaks do not appear at the longitudinal plate wavenumber, they do appear in the correct general region. Additionally, we have only used *representative* figures for the dimensions, and under certain sonar dome geometries the wavenumbers at which resonance occurs may be different.

The other candidate for the explanation of the signals is that identified in the course of the analysis of the finite plate. Applied pressure varying sinusoidally with wavenumber equal to the bending wavenumber of the plate induces vibrations in the plate which are a superposition of several monochromatic vibrations. However, only those vibrations which are supersonic with respect to the fluid are transmitted at full strength to the hydrophones. This phenomenon is a plausible explanation of the problem, although when viscoelastic effects are taken into account, the peak due to this effect in the case of a finite plate with a rigid boundary is lower than that for resonant effects. This behaviour is worth investigating further, however, since more sophisticated models of the sonar dome could show an increased effect — the vibrations induced in the finite plate are strongly dependent on its dimensions.

## 6.2 Further Research

While we have identified the probable mechanisms by which vibrations are transmitted through the sonar dome at particular wavenumbers, a study of more accurate models of the sonar dome is needed in order to confirm these. In particular, it will become necessary to consider finite structures in three dimensions, as opposed to the two-dimensional finite structures analysed in this project.

Such models will undoubtedly require some numerical methods in order to find a solution, because the detailed geometry is not simple. It would be possible to use a package such as FastFlo or the Matlab PDE toolbox for two-dimensional geometries, but in three dimensions these would be more difficult to implement, and slower to run. The alternative of using ray theory would be acceptable for the acoustics in the water, but in the dome we have  $kH \approx 0.65$ , which is too small for the theory to be appropriate here.

# Appendix A

## Graphs

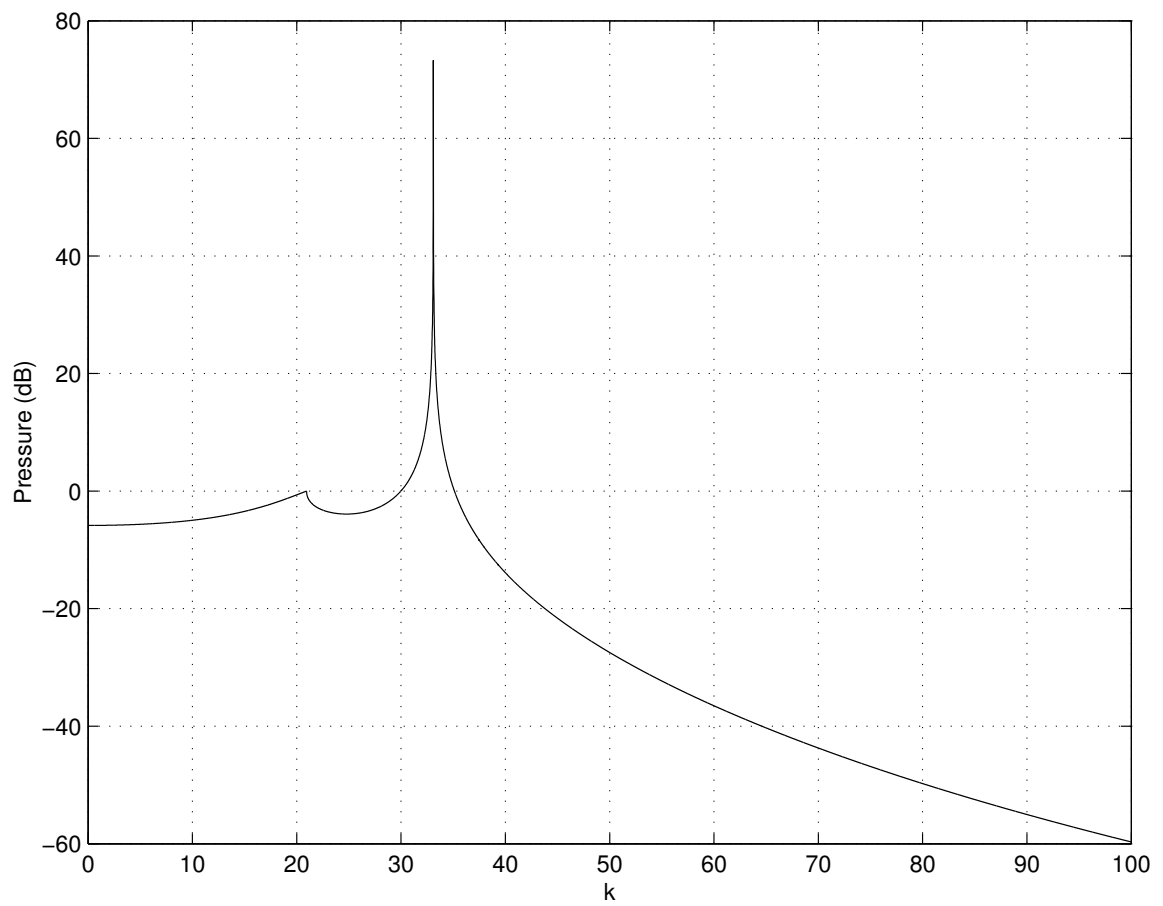


Figure A.1: Graph of the pressure on the lower side of a thin plate as a function of the excitation wavenumber

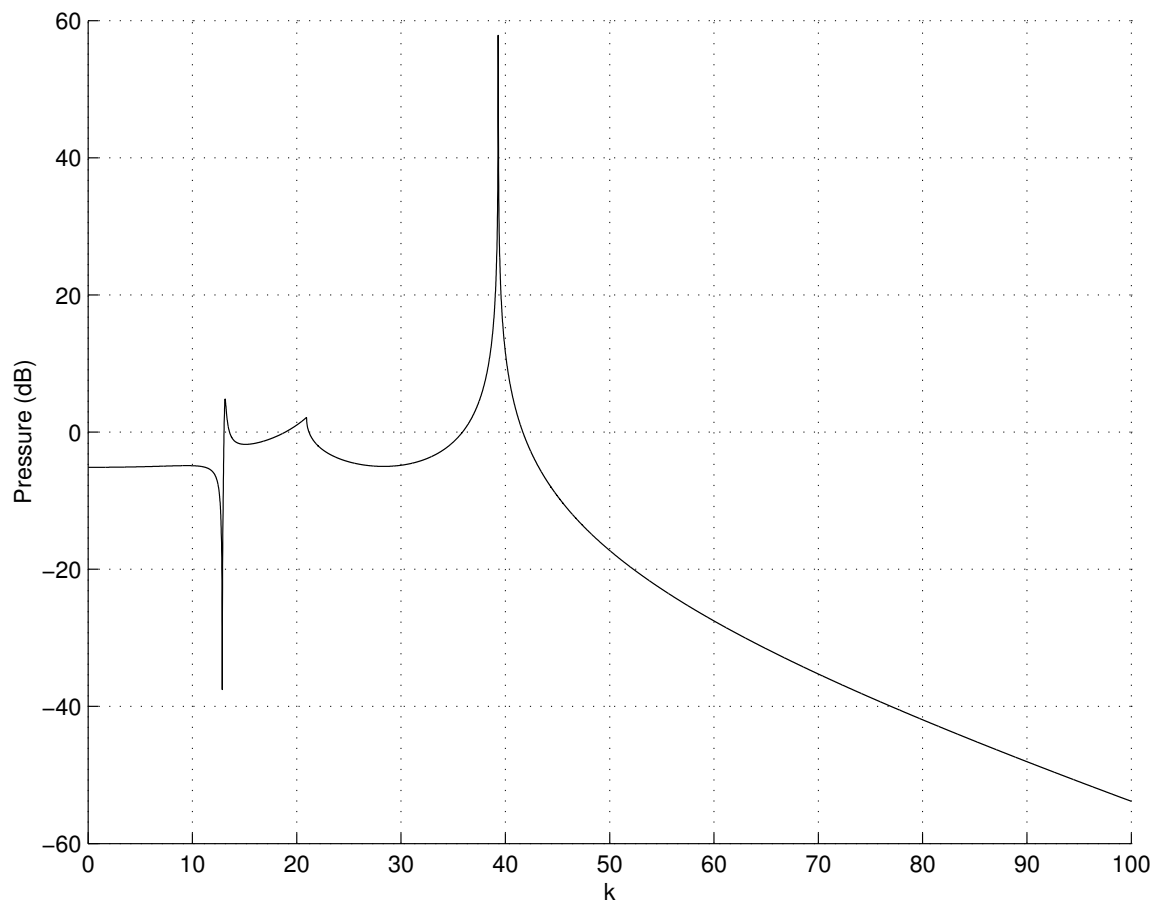


Figure A.2: Graph of the pressure on the lower side of a thick plate as a function of the excitation wavenumber

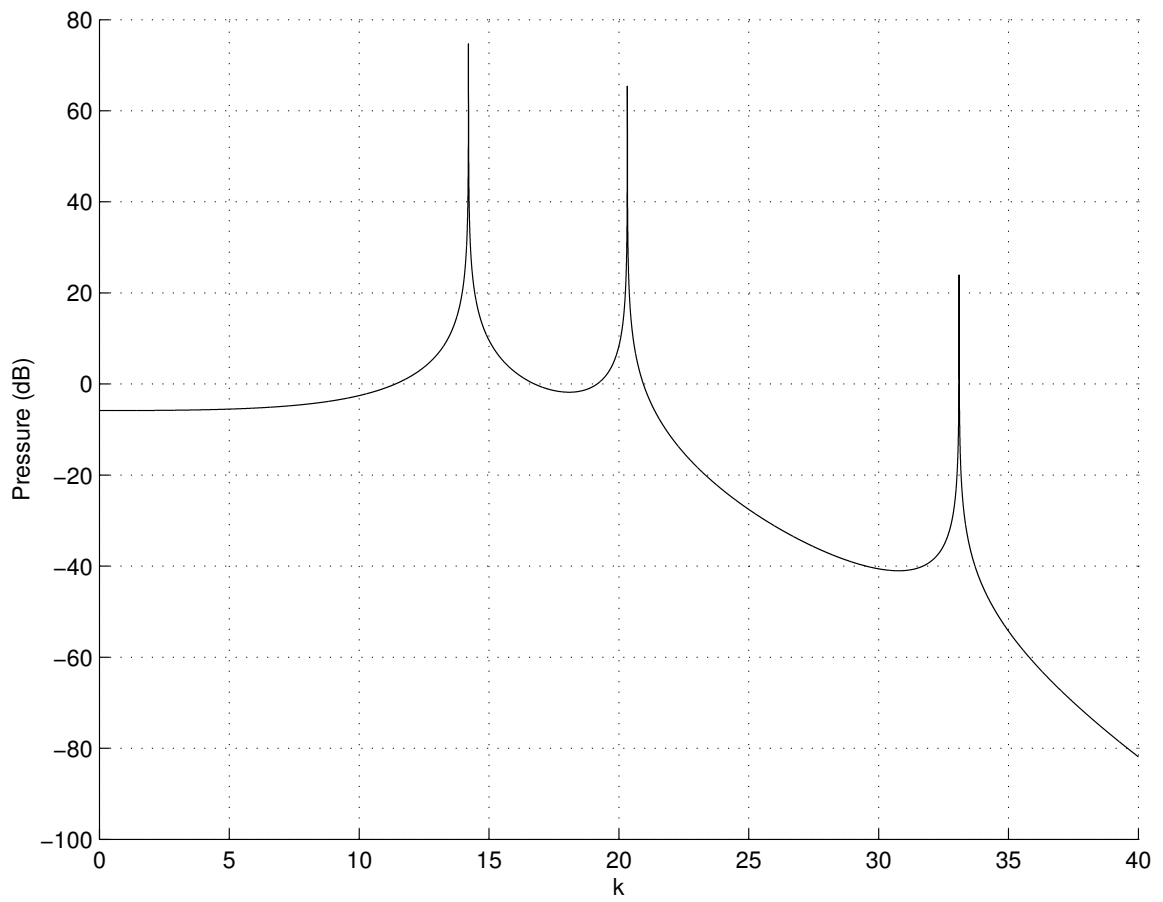


Figure A.3: Graph of the pressure measured at a distance  $h_0$  from a thin plate, with a rigid boundary

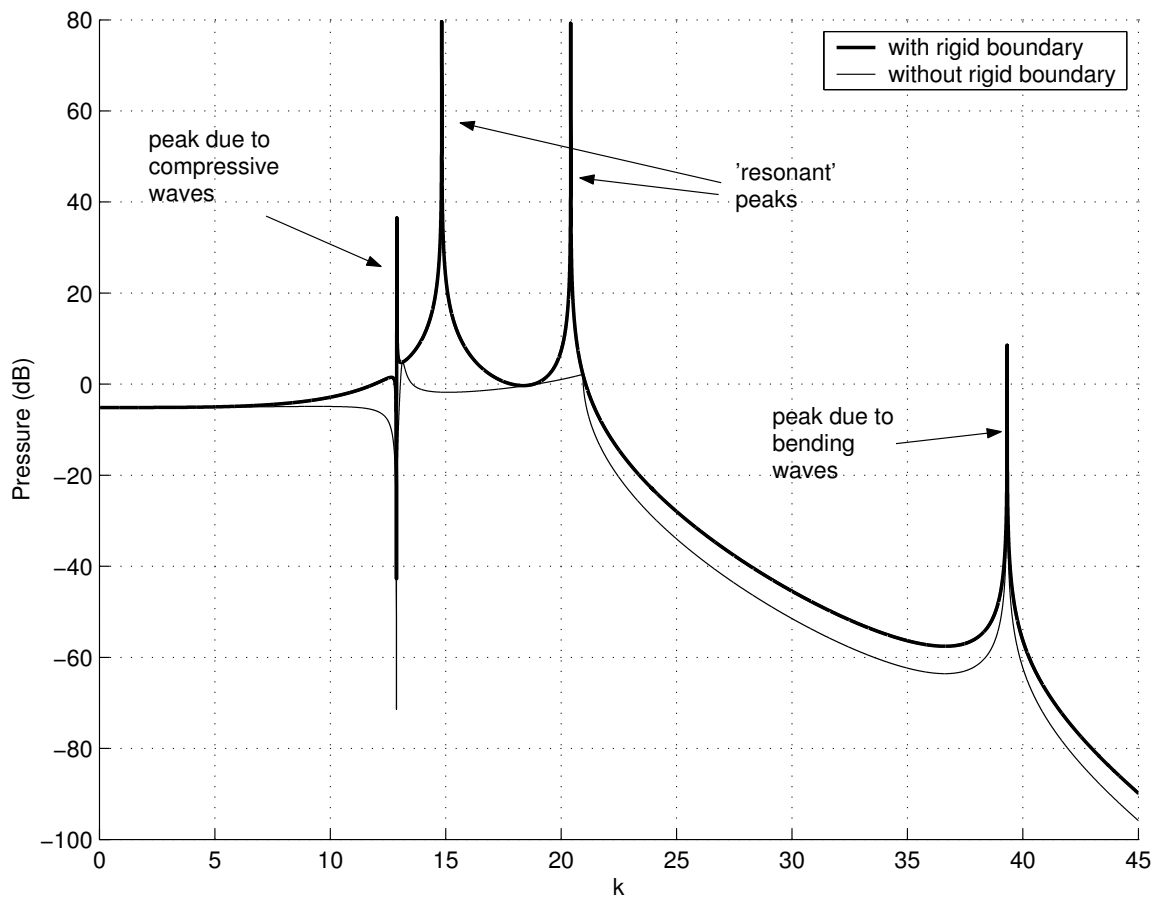


Figure A.4: Graph of the pressure measured at a distance  $h_0$  from a thick plate, with and without a rigid boundary

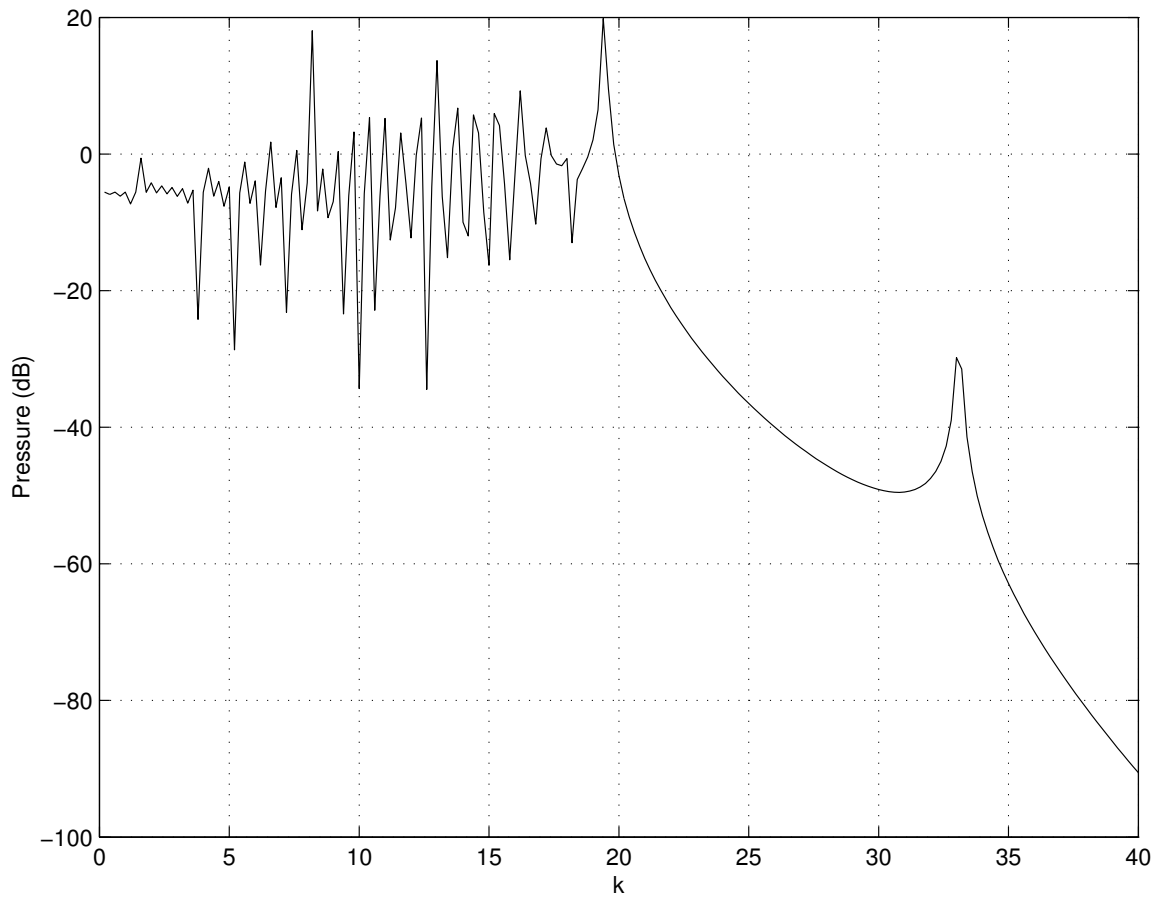


Figure A.5: Graph of the pressure at a distance  $h_0$  inside a thin cylindrical shell in dB as a function of the excitation wavenumber

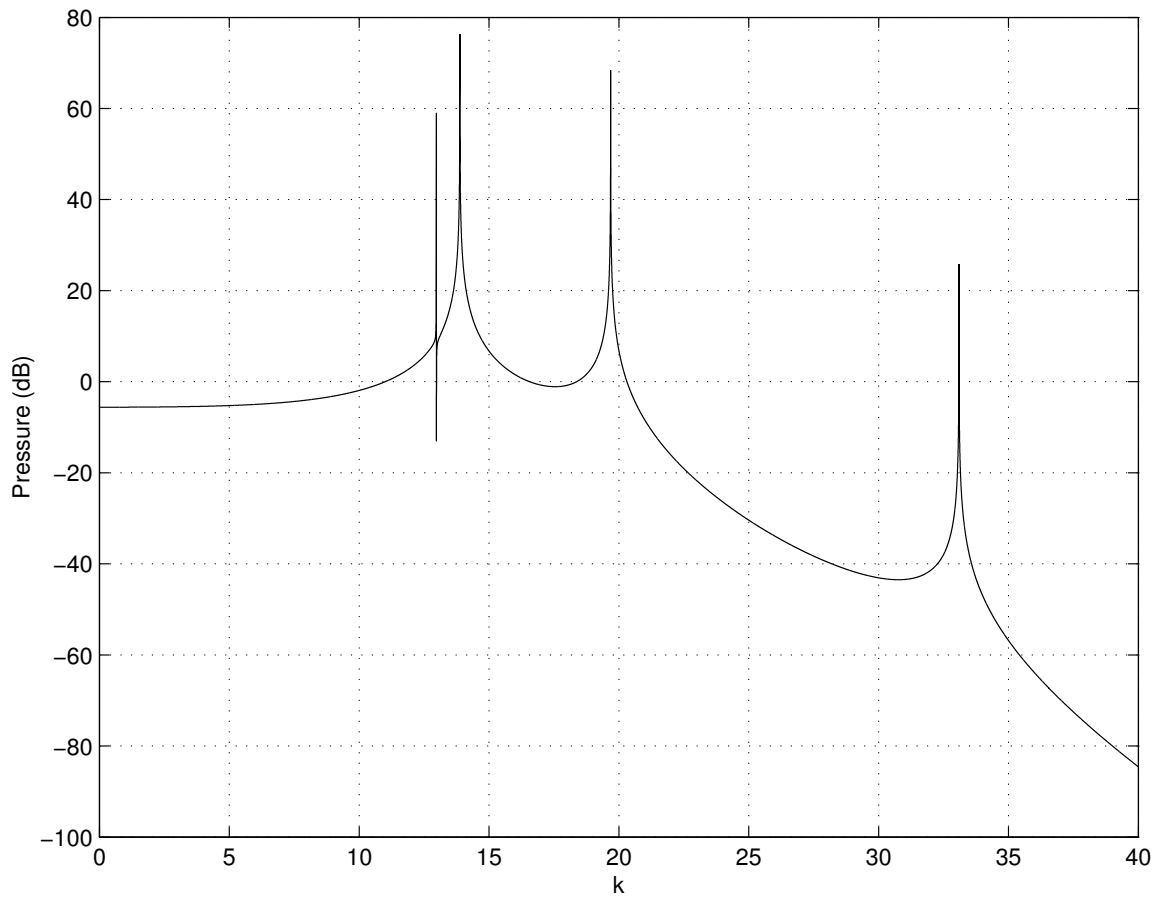


Figure A.6: Graph of the pressure inside a thin cylindrical shell on a rigid cylinder, in dB as a function of the excitation wavenumber

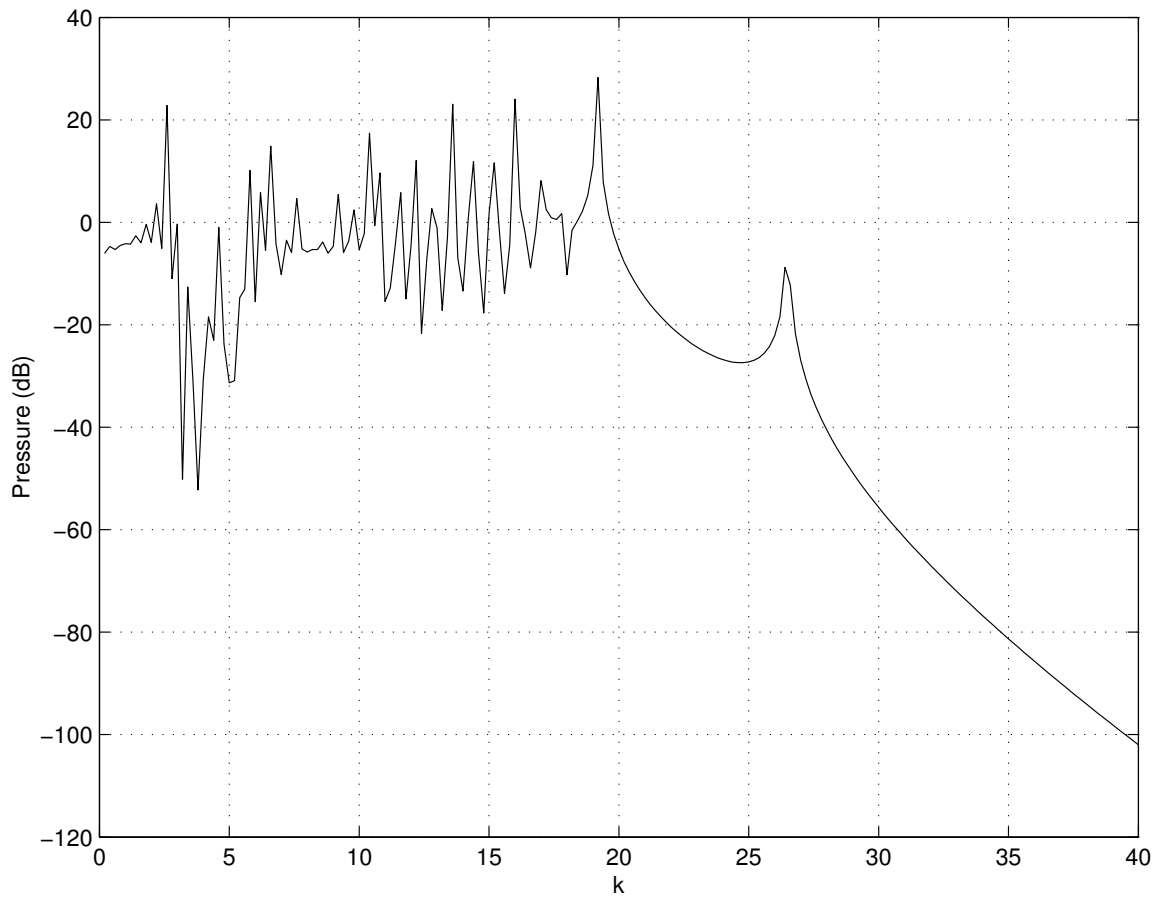


Figure A.7: Graph of the pressure at a distance  $h_0$  inside a thick cylindrical shell as a function of the excitation wavenumber

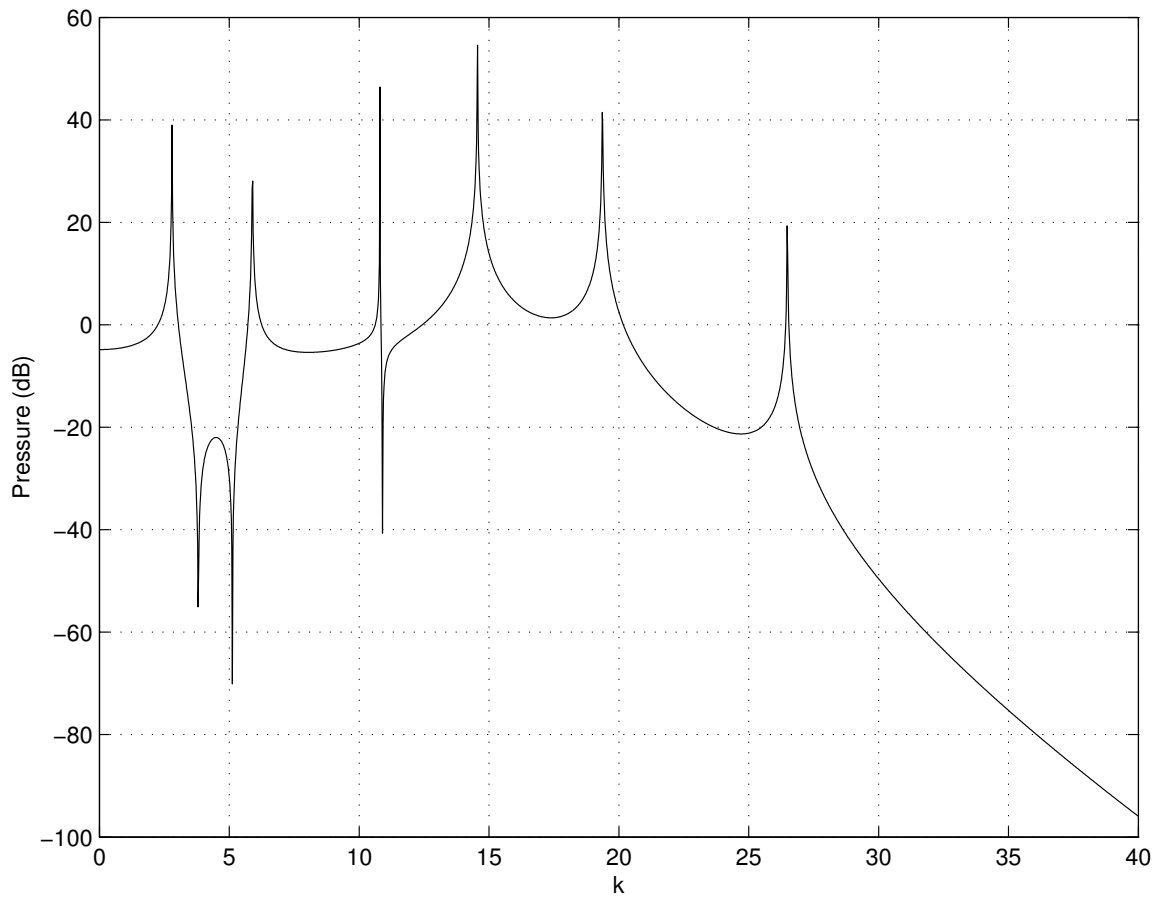


Figure A.8: Graph of the pressure inside a thick cylindrical shell on a rigid cylinder, as a function of the excitation wavenumber

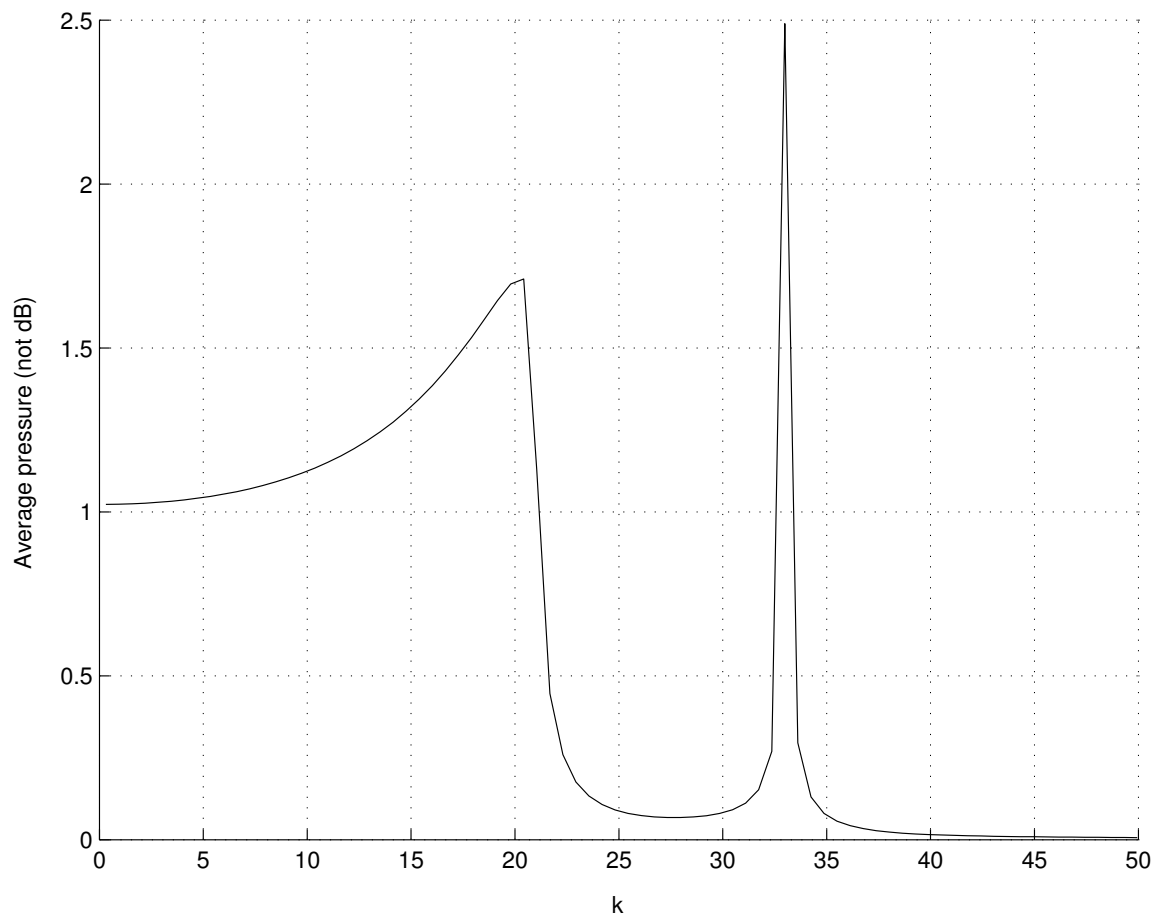


Figure A.9: Graph of the pressure at a distance  $h_0$  behind a thin finite plate, as a function of the excitation wavenumber

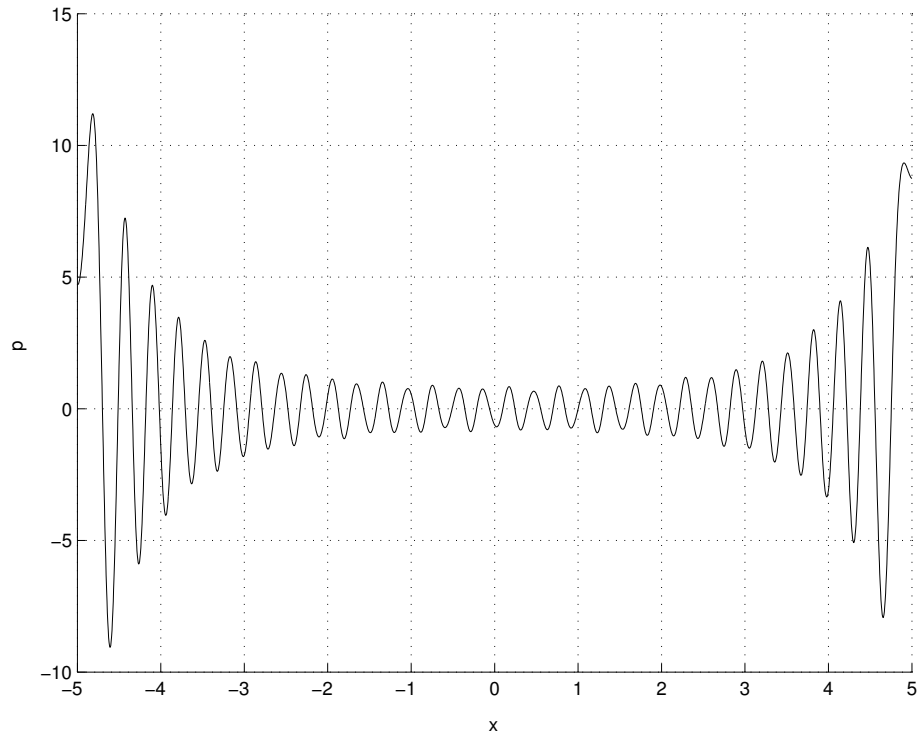


Figure A.10: Graph of the pressure at a distance  $h_0$  behind a thin finite plate, at  $k = 33.99 \text{ m}^{-1}$

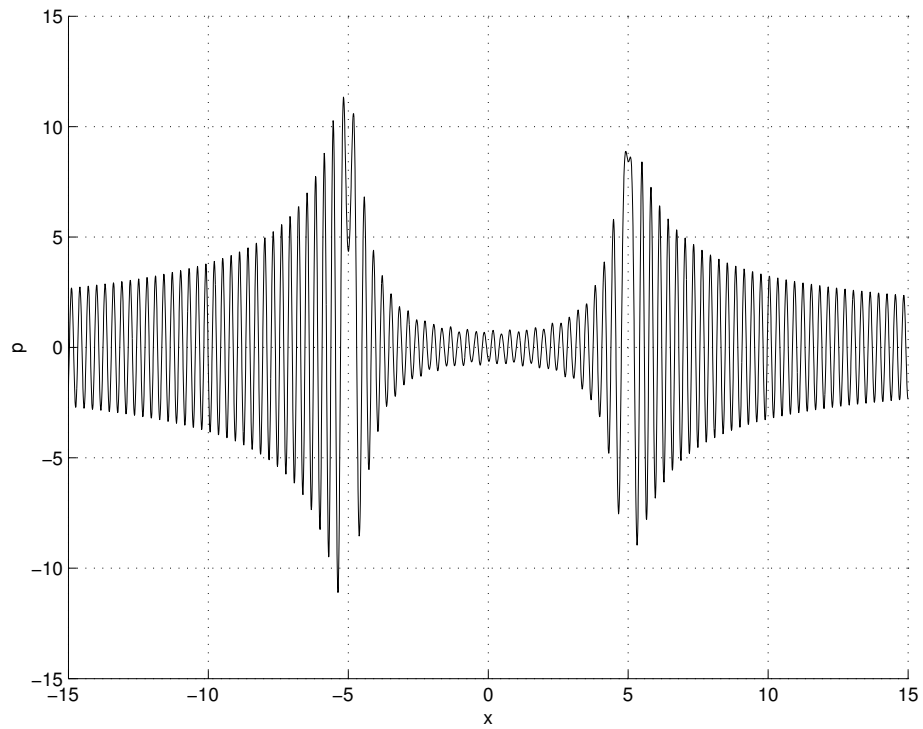


Figure A.11: Graph of the pressure at a distance  $h_0$  behind a thin finite plate, at  $k = 33.99 \text{ m}^{-1}$ , outside  $[-l, l]$

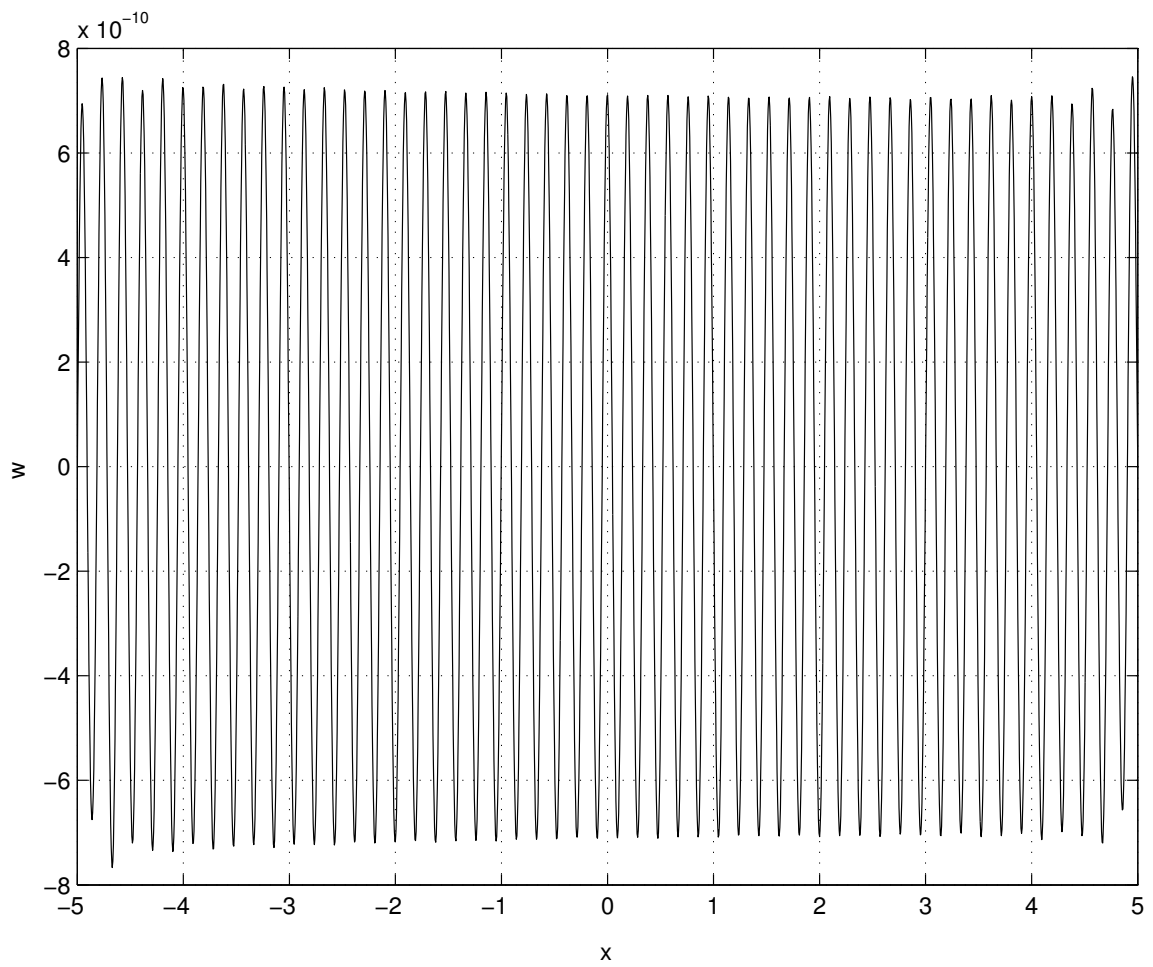


Figure A.12: Graph of the thin finite plate displacement, at  $k = 33.99 \text{ m}^{-1}$

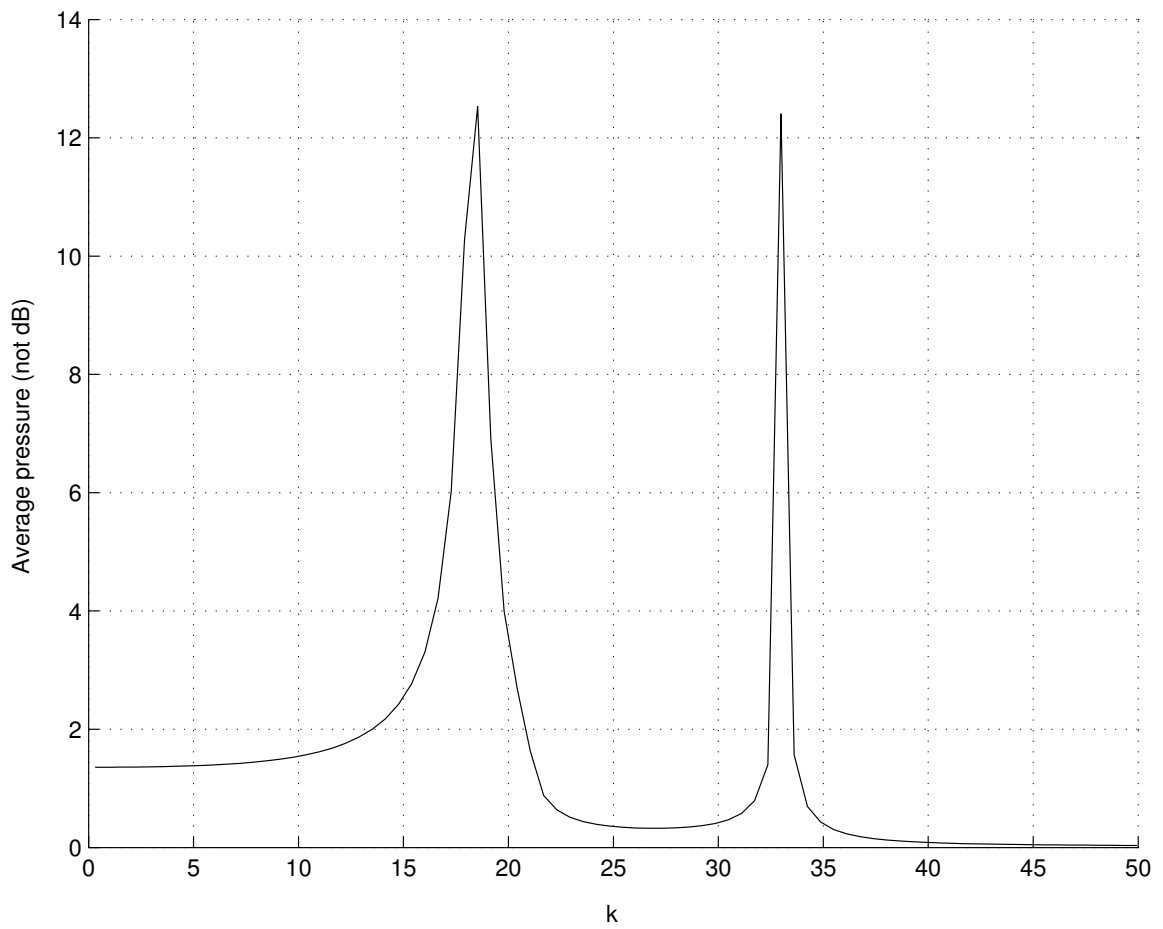


Figure A.13: Graph of the pressure at a distance  $h_0$  behind a thin finite plate on a rigid boundary, as a function of the excitation wavenumber

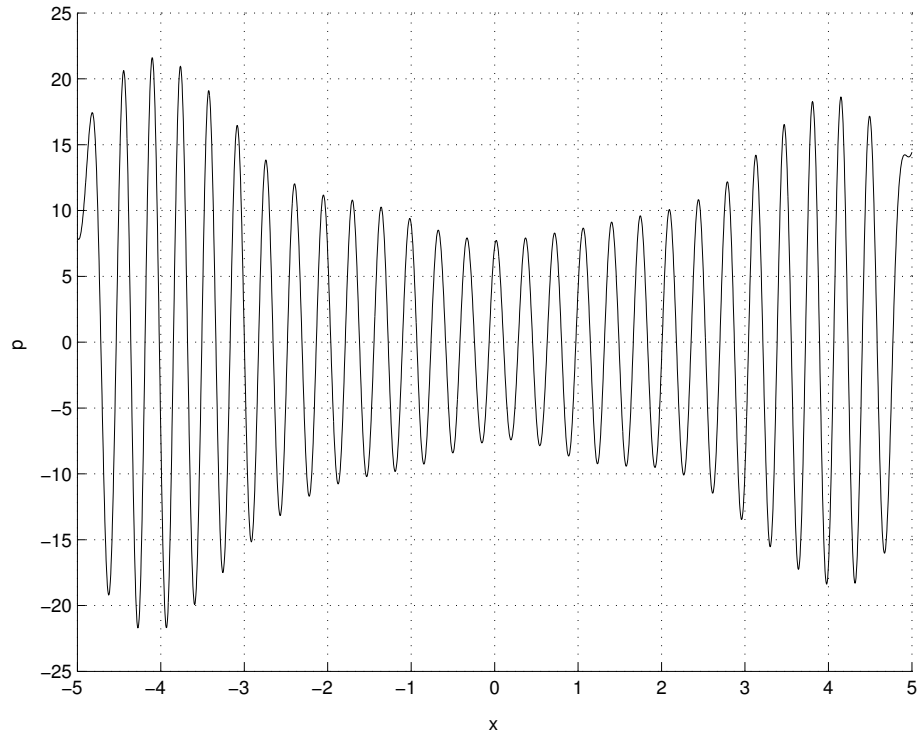


Figure A.14: Graph of the pressure at a distance  $h_0$  behind a thin finite plate on a rigid boundary, at  $k = 33.99 \text{ m}^{-1}$

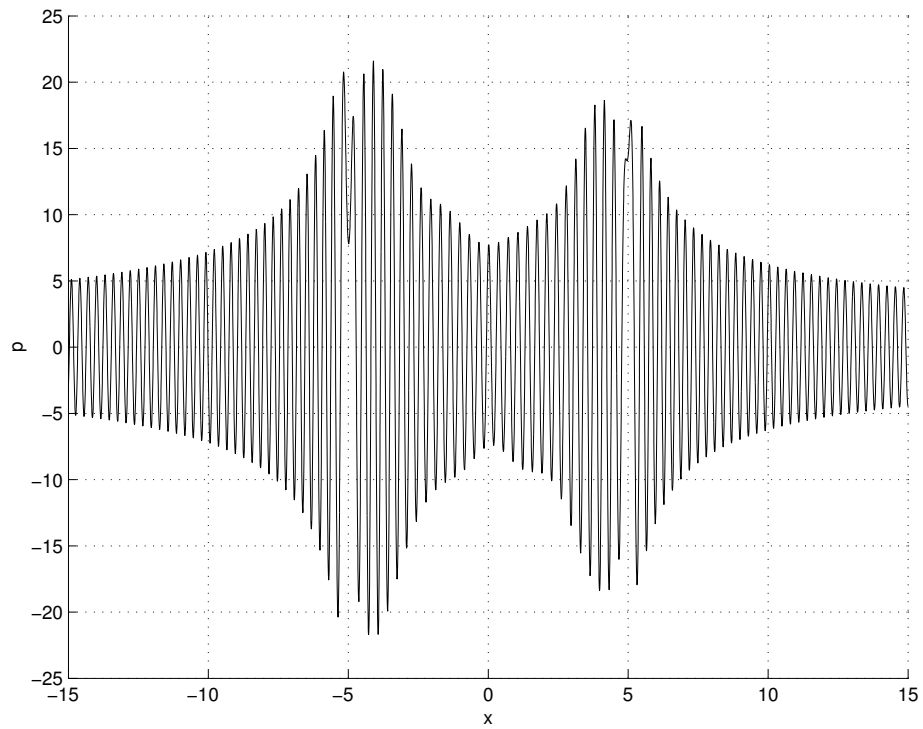


Figure A.15: Graph of the pressure at a distance  $h_0$  behind a thin finite plate on a rigid boundary, at  $k = 33.99 \text{ m}^{-1}$ , outside  $[-l, l]$

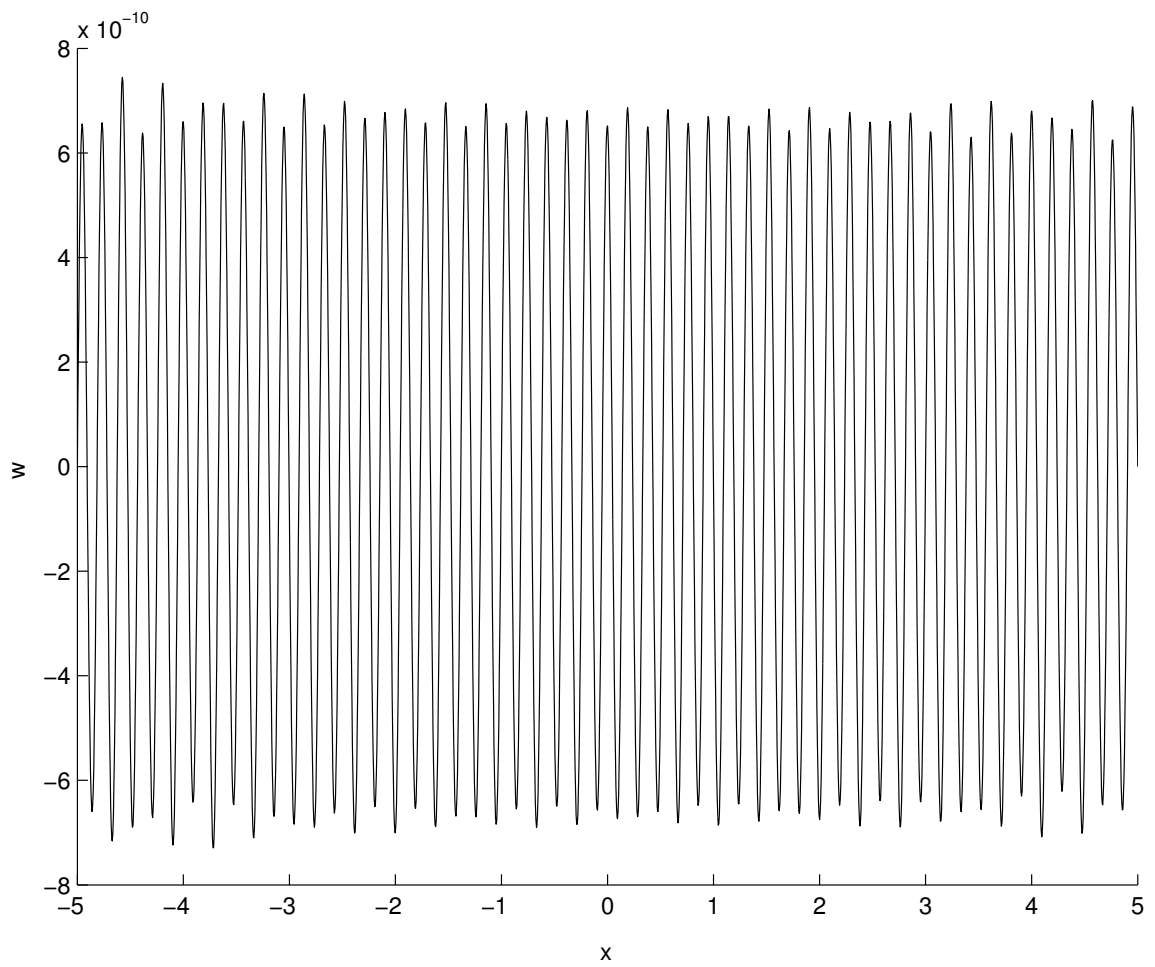


Figure A.16: Graph of the thin finite plate displacement with a rigid boundary, at  $k = 33.99 \text{ m}^{-1}$

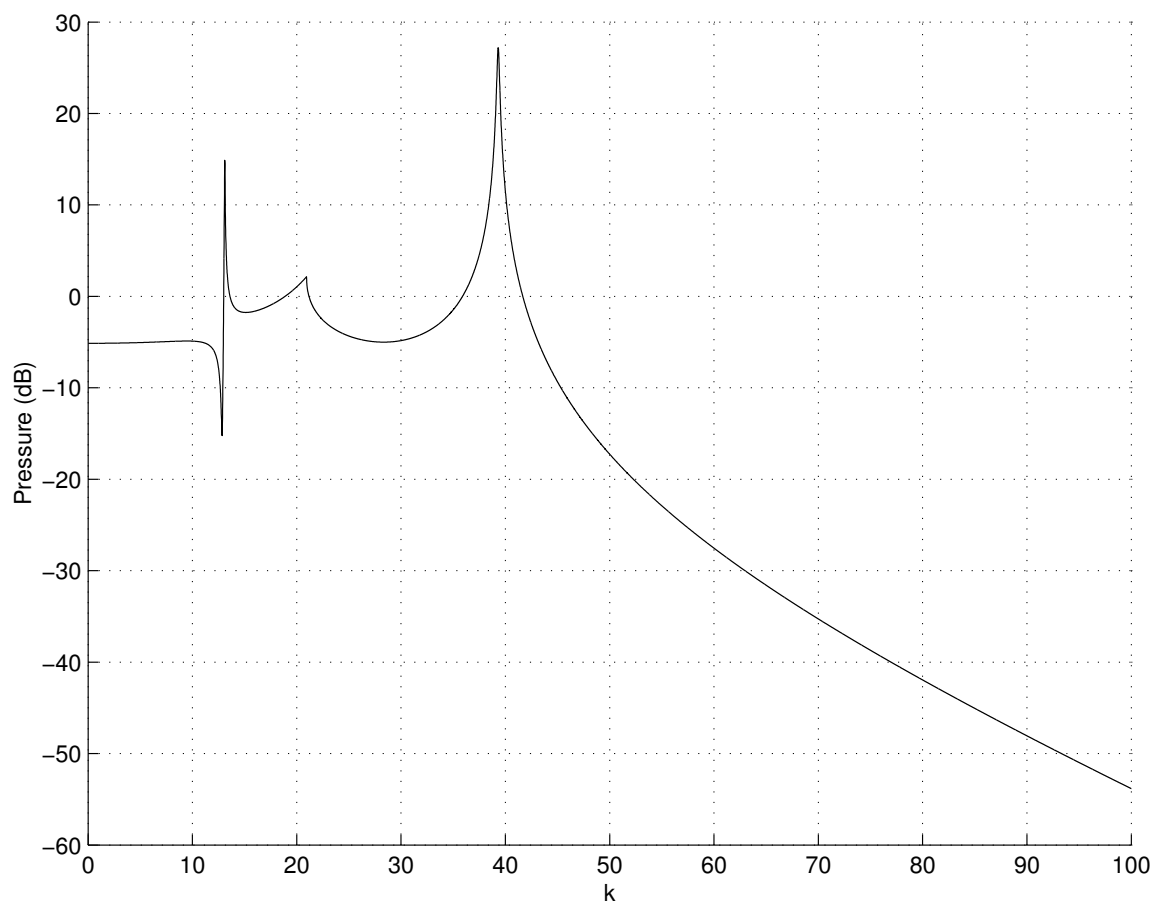


Figure A.17: Graph of the pressure on the lower side of a thick plate as a function of the excitation wavenumber; with complex elastic moduli

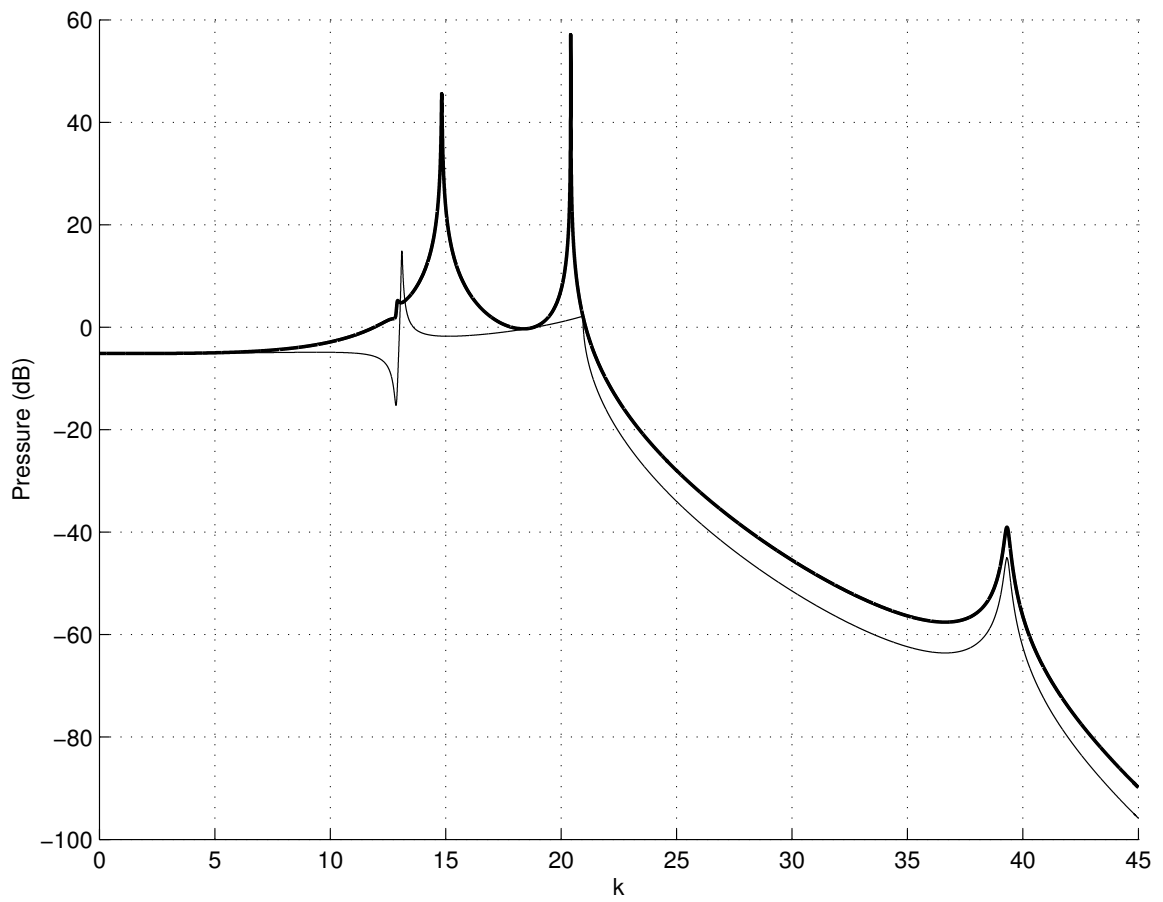


Figure A.18: Graph of the pressure measured at a distance  $h_0$  from a thick plate, with and without a rigid boundary; with complex elastic moduli

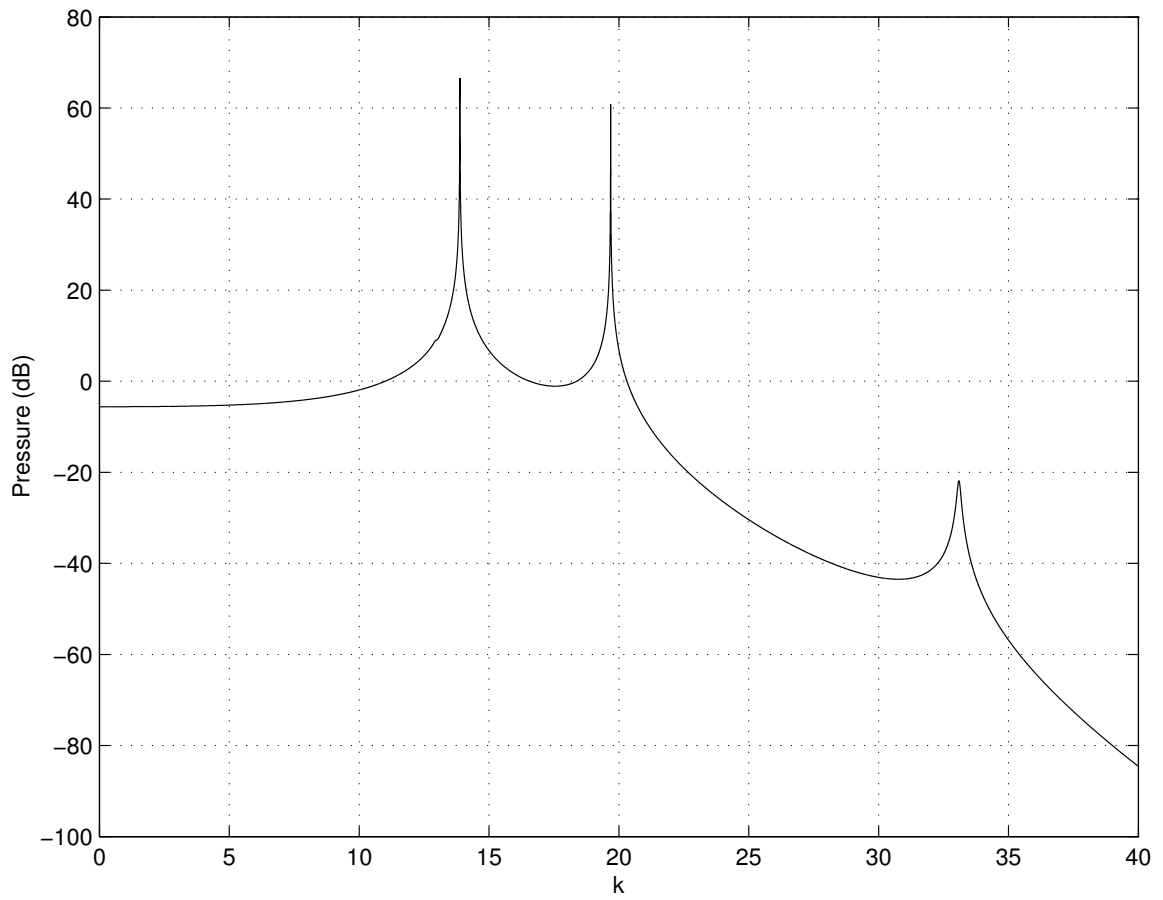


Figure A.19: Graph of the pressure at a distance  $h_0$  inside a thin cylindrical shell on a rigid cylinder, in dB as a function of the excitation wavenumber; with complex elastic moduli

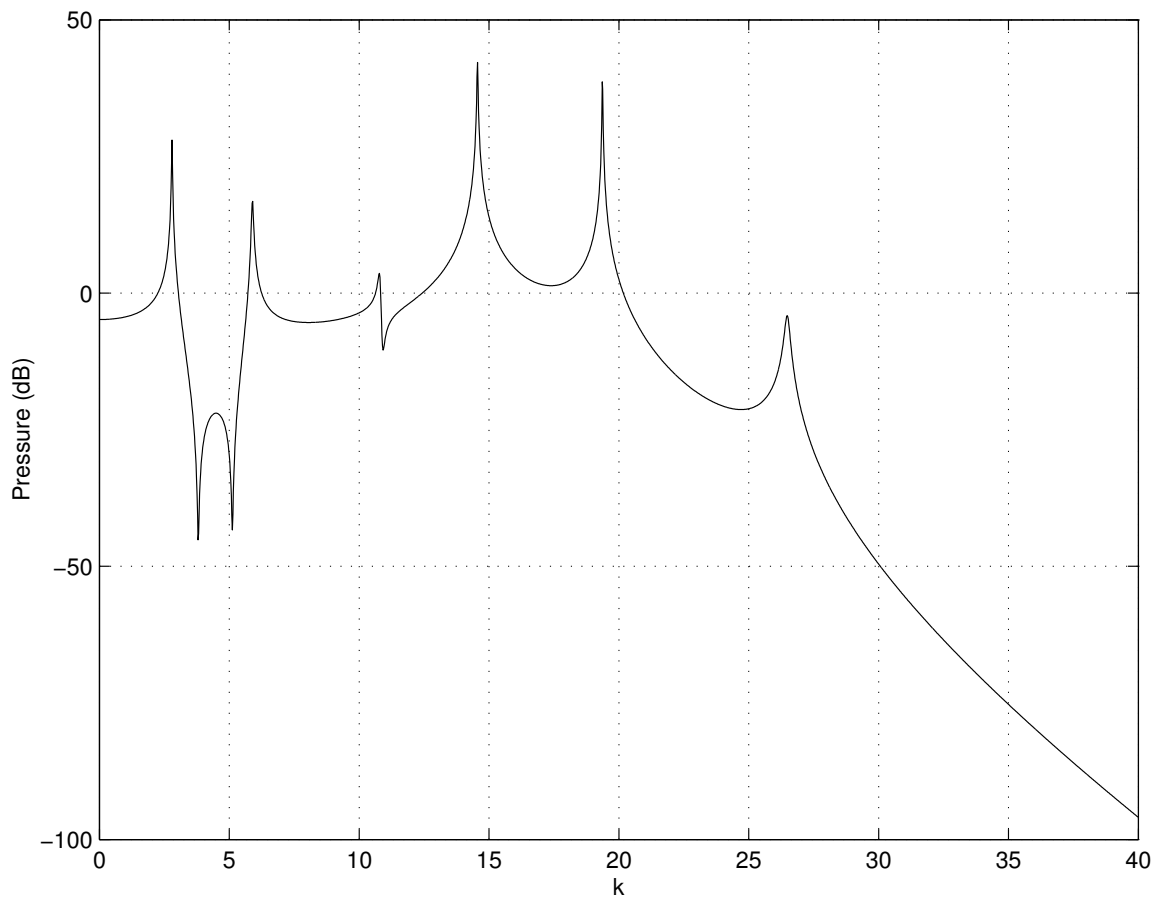


Figure A.20: Graph of the pressure at a distance  $h_0$  inside a thick cylindrical shell on a rigid cylinder, as a function of the excitation wavenumber; with complex elastic moduli

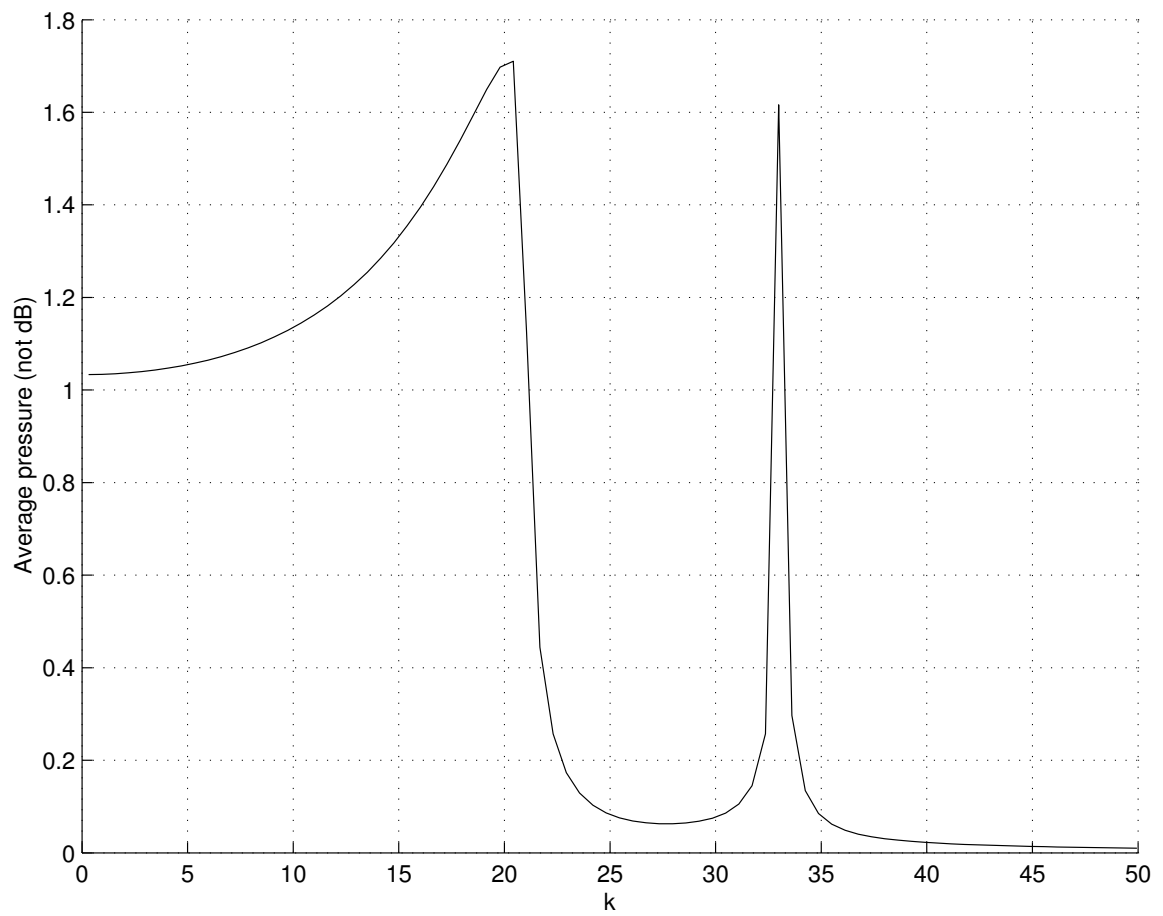


Figure A.21: Graph of the pressure at a distance  $h_0$  behind a thin finite plate, as a function of the excitation wavenumber; with complex elastic moduli

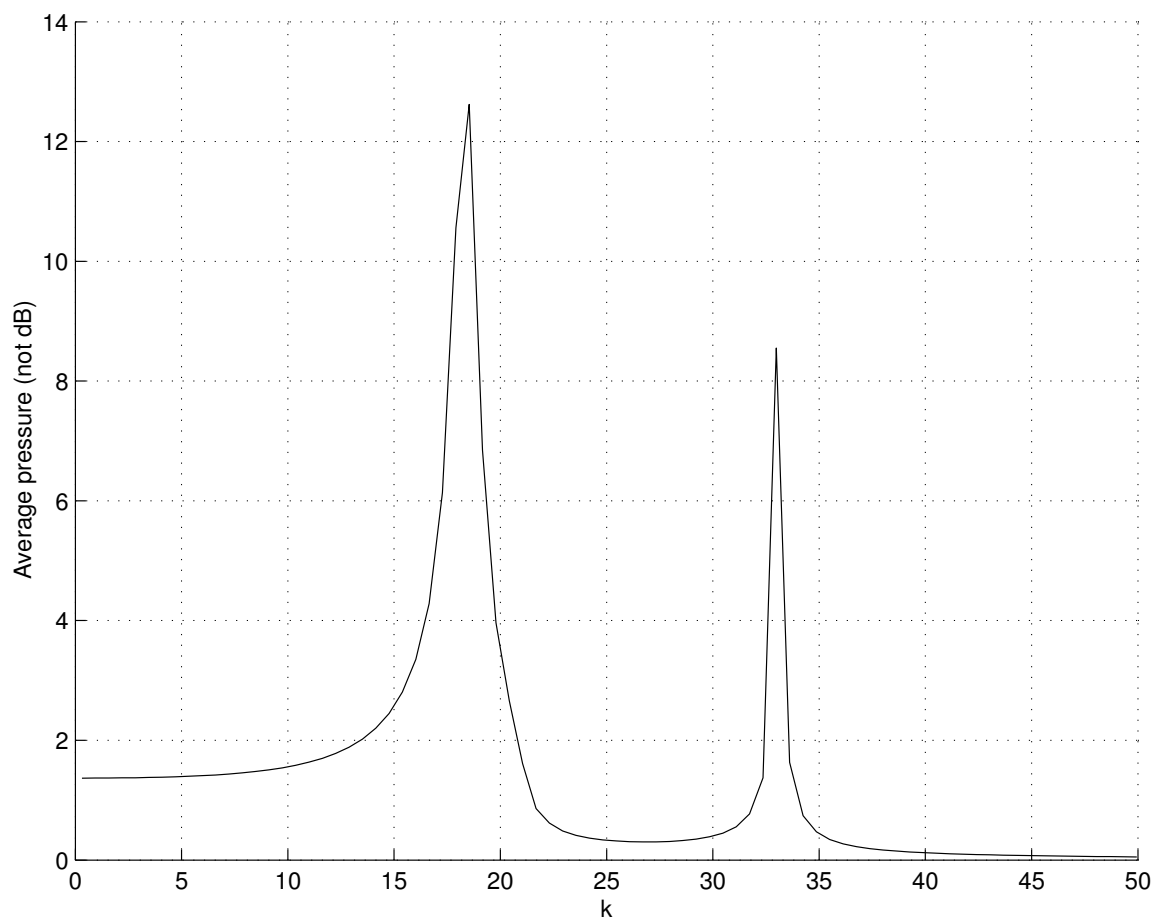


Figure A.22: Graph of the pressure at a distance  $h_0$  behind a thin finite plate with a rigid boundary, as a function of the excitation wavenumber; with complex elastic moduli

# References

- [1] M. ABRAMOWITZ AND I.A. STEGUN. *Handbook of Mathematical Functions*. Wiley, 1972.
- [2] D.J. ACHESON. *Elementary Fluid Dynamics*. Oxford University Press, 1990.
- [3] D.E. BOURNE AND P.C. KENDALL. *Vector Analysis and Cartesian Tensors*. Stanley Thornes, third edition, 1992.
- [4] L.M. BREKHOVSKIKH. *Waves in Layered Media*. Academic Press, second edition, 1980.
- [5] L. CREMER, M. HECKL, AND E.E. UNGAR. *Structure-borne Sound*. Springer-Verlag, 1973.
- [6] D.G. CRIGHTON AND D. INNES. The modes, resonances and forced response of elastic structures under heavy fluid loading. *Phil. Trans. R. Soc. Lond., Ser. A*, **312**:295–341, 1984.
- [7] D.C. GAZIS. Three-dimensional investigation of the propagation of waves in hollow circular cylinders, part 1. *J. Acoust. Soc. America*, **31**(5):568–573, 1959.
- [8] M.C. JUNGER AND D. FEIT. *Sound, Structures and their Interaction*. MIT Press, second edition, 1986.
- [9] L.D. LANDAU AND E.M. LIFSHITZ. *Theory of Elasticity*. Pergamon, second edition, 1970.
- [10] A.W. LEISSA. *Vibration Of Shells*. NASA, 1973.
- [11] M.J. LIGHTHILL. *Fourier Analysis and Generalised Functions*. Cambridge University Press, 1958.
- [12] A.E.H. LOVE. *A Treatise On The Mathematical Theory Of Elasticity*. Fourth edition, 1927. Reprinted by Dover, 1944.
- [13] I. MIRSKY. Wave propagation in transversely isotropic circular cylinders, part 1. *J. Acoust. Soc. America*, **37**(6):1016–1021, 1965.
- [14] A.C. PIPKIN. *Lectures on Viscoelasticity Theory*. Springer-Verlag, 1972.
- [15] J.W.S. RAYLEIGH. On the free vibrations of an infinite plate of homogeneous isotropic elastic matter. *Proc. Lond. Math. Soc.*, **20**:225–234, 1889.

- [16] J.W.S. RAYLEIGH. *The Theory of Sound, Vol. 1*. Second edition, 1894–1896. Reprinted by Dover, 1945.
- [17] E.A. SKELTON AND J.H. JAMES. *Theoretical Acoustics of Underwater Structures*. Imperial College Press, 1997.
- [18] THALES UNDERWATER SYSTEMS. *Flow Excitation of a Finite Curved Elastic Plate*. MSc project presentation, Phil Cotterill, 17th March 2003.
- [19] A.B. TAYLER. *Mathematical Models in Applied Mechanics*. Oxford University Press, 1986.
- [20] S. ZHANG AND J. JIN. *Computation of Special Functions*. Wiley, 1996.